Information Fusion 90 (2023) 298–315

Contents lists available at ScienceDirect

Information Fusion

journal homepage: www.elsevier.com/locate/inffus

Full length article

A sensor fusion approach to MARG module orientation estimation for a real-time hand tracking application

Neeranut Ratchatanantakit *, Nonnarit O-larnnithipong, Pontakorn Sonchan, Malek Adjouadi, Armando Barreto

Department of Electrical and Computer Engineering, Florida International University, 10555 W Flagler St., Miami, 33174, FL, USA

ARTICLE INFO

Keywords:
Dead reckoning
MARG
Inertial measurement unit
Gyroscope drift
Drift correction algorithm
Quaternion correction
Magnetic distortion
Hand motion tracking

ABSTRACT

This paper introduces a new algorithm (Gravity & Magnetic North Vector correction — Double SLERP, or "GMV-D") to estimate the orientation of a MEMS Magnetic/Angular-Rate/Gravity (MARG) sensor module using sensor fusion in the context of a real-time hand tracking application, for human–computer interaction purposes.

Integrated MEMS MARG modules are affordable, small, light and consume minimal power. As such, there is interest in using them for monitoring the orientation of various body segments, to which they can be attached (e.g., the finger segments of a gloved hand). However, each of the 3 types of signals they provide has proven insufficient to yield robust orientation estimates, particularly in regions of space where the geomagnetic field is distorted. The significance (main contribution) of the approach we present is the computation of a final orientation estimate that uses all the signals generated by inexpensive (e.g., less than 20 USD, in large quantities) integrated MEMS MARG modules but weighs their contributions with simple, real-time-updatable parameters that prevent erroneous corrections when the pre-conditions for their valid use are not met. This will enable the use of inexpensive integrated MEMS MARG modules for hand tracking applications in human–computer interaction and other areas of work where tracking the orientation of body segments in real-time is important.

In each iteration, GMV-D defines an initial orientation estimate from integration of gyroscopic signals ("dead reckoning"), and also calculates accelerometer-based and magnetometer-based corrections. These corrections are defined on the assumptions that the module is near static and affected by an undistorted geomagnetic field.

Because these assumptions are seldom fully met simultaneously, the information fusion challenge is to apply each correction only to the extent that its corresponding pre-conditions are met, as inappropriate corrections will introduce significant error in the future orientation estimates. To achieve this, GMV-D develops an accelerometer correction trustworthiness parameter, $0 \leq \alpha \leq 1$, and a magnetometer correction trustworthiness parameter, $0 \leq \mu \leq 1$, both of which are updated on a sample-by-sample basis and are available at each iteration of the algorithm. The information fusion phase of the algorithm implements the corrections in a two-tiered application of Spherical Linear Interpolation (SLERP) of the quaternions representing the initial dead reckoning estimate and the available corrections, scaled according to their corresponding levels of trustworthiness.

GMV-D was evaluated in comparison to 2 other orientation correction approaches (Kalman Filtering and GMV-S) and contrasted with 2 contemporary complementary filter approaches (Madgwick , Mahony). The results confirm that GMV-D displayed better orientation estimation performance when the algorithms operated in an area with known distortion of the geomagnetic field.

1. Introduction

Today, computers are part of many aspects of human activity and users seek to interact with computers in ways that are natural and intuitive. The popularity of Virtual Reality (VR) and Augmented Reality (AR) has increased in many applications [1]. In this current context, it would be highly beneficial for computer systems to have the real-time ability of capturing user hand movement in terms of both position and orientation. Currently available input devices like mice, game

* Corresponding author.
E-mail address: neeranut.ratch@gmail.com (N. Ratchatanantakit).

https://doi.org/10.1016/j.inffus.2022.09.017
Received 10 November 2021; Received in revised form 6 June 2022; Accepted 20 September 2022
Available online 24 September 2022

pads, joysticks and wands, require the user to perform highly artificial sequences of actions. In contrast, hand motion tracking can be used to implement a more intuitive way to provide input to the computer and to give the computer a mechanism to gauge the user's body language. Thus, an improvement in the computer's capability to perform real-time hand tracking may be a crucial step towards the development of the next generation of human–computer interaction systems.

When Micro Electro-Mechanical Systems (MEMS) accelerometers (1990's) and gyroscopes (2000's) became commercially available, some in the Human–Computer Interaction (HCI) community envisioned attaching them to segments of the body (e.g., the finger segments, embedding the miniature sensors in a glove) to track them in a manner similar to the tracking of aircraft equipped with aeronautical inertial sensors (accelerometers, gyroscopes). However, that goal is not yet fully realized due to the much poorer performance characteristics of the MEMS gyroscopes and accelerometers in comparison to the performance of their aeronautical counterparts [2]. A direct re-utilization of the processing techniques used for monitoring the navigation of large vehicles has proven inefficient for robust orientation estimation of MEMS Inertial Measurement Units (IMUs), which contain gyroscopes and accelerometers or Magnetic/Angular-Rate/Gravity (MARG) modules, which contain, in addition, magnetometers. Therefore, the motivation of our work was to develop a novel real-time orientation estimation algorithm that uses all the signals available from the MARG module but avoids the execution of costly erroneous corrections, which degrade the orientation estimates for multiple iterations into the future.

In this initial development we have studied the use of a single MARG module (Yost Labs 3-Space Sensor) attached to a small wooden rectangular prism. This facilitates placing the sensor in repeatable orthogonal poses. Furthermore, we have used the MARG module in conjunction with a 3-camera IR-video tracking system (OptiTrack V120 Trio) that provides position coordinates of the MARG sensor.

The remainder of this introduction will describe the context in which we approach the MARG orientation estimation problem and the most significant previous developments in this area. This overview will provide context for the identification of key contributions (e.g., definition of scalar accelerometer and magnetometer trustworthiness parameters that are adapted with every iteration and progressive mapping of magnetically disturbed areas) to be described in further detail in the Discussion section.

1.1. Specification of the context and technical challenge

There have been multiple efforts to derive reliable estimates of orientation from MEMS MARG modules. These modules have also been called Magnetic and Inertial Measurement Units (MIMUs), as they contain a 3-axis accelerometer, a 3-axis rate gyroscope as well as a 3-axis-magnetometer, which are said to give these sensor modules (3 + 3 + 3) "9 degrees of freedom" (or "nine axes"). A comprehensive survey of the techniques for this purpose developed over the last 40 years is offered by Nazarahari and Rouhani [3].

However, we have sought to address the challenge of real-time orientation estimation from MARG modules attached to an instrumented glove, for the specific goal of human–computer interaction. Prospectively, MARG modules will be attached to the proximal and middle phalanges and to the dorsal surface of the glove, to monitor their orientations. The success of this approach, however, requires that reliable orientation estimates be obtained from each one of the MARG modules. Given that context, we have developed a MARG orientation estimation solution within the following constraints:

C1 - The instrumented glove will be used in the vicinity of the computer. This means that (*C1a*) it is feasible to use a multi-camera video system to obtain an approximate estimate of the position of a segment (e.g., the wrist) of the hand of the user. It also means that (*C1b*) the location of any object (particularly large ferromagnetic objects) within the working space of the system is likely to be constant or change slowly.

C2 - The (gloved) hand of a human subject interacting with a computer system will typically experience frequent static episodes, in between purposeful movements and gestures.

1.2. Three sources of information

Each of the 3 sensor modalities in a MARG module provides information that may be used to help estimate the module's orientation. However, each modality faces specific and important limitations.

The 3-axis rate gyroscope in the MARG module provides periodical measurements of the angular velocity of the module in each axis, and, in principle, it could, by means of accumulation (i.e., numerical integration), calculate the total orientation change experienced by the module from its initial orientation.

Unfortunately, different types of gyroscopes have different accuracy levels that tend to be in proportion to their price [2], from navigation systems in aviation to the MEMS gyroscopes used in portable devices (e.g., the prospective instrumented glove). MEMS gyroscopes offer the lowest performance, typically including significant offset levels in their outputs, which, furthermore, may not be exactly constant, but instead, may be slowly varying. If the "bias offset error" in angular velocity persists, it will generate the "drift" error in the orientation estimates defined by integration, which, left uncorrected, could soon render those estimates useless. In traditional inertial navigation systems, the inertial estimates of orientation and position are usually corrected periodically using information from external sources, such as Global Positioning System (GPS) information. However, GPS is not a viable option for our indoor target application.

In contrast to the continuous accumulation method that must be used to determine orientation from angular rate measurements (which is also called "dead reckoning"), both accelerometers and magnetometers could, potentially, provide information to aid in the estimation of the orientation of the module using instantaneous measurements only. However, the approach is predicated on the assumption that the vector field that each sensor measures is uniform at all times and in all locations within the operating space of the device. This assumption is typically not completely and/or permanently fulfilled in most practical scenarios.

If the only acceleration detected by the 3 accelerometer axes were the acceleration of gravity ($g = 9.81\ m/s^2$), we would leverage the fact that the acceleration vector is always oriented vertically, pointing downwards (towards the floor). Therefore, the readings from the 3 orthogonal axes of the MARG module, at any given time, would have to be a decomposition of the vertical acceleration of gravity along the 3 orthogonal directions in which the accelerometer axes sense that gravity. In general, if gravity were the only acceleration at play, reading the instantaneous accelerometer outputs would constitute "an observation" of the gravity vector. While observing the gravity vector alone cannot uniquely determine 3-dimensional orientation [4], such readings would provide a sound way to confirm or correct an orientation estimate derived from a different source of information (e.g., the gyroscope signals, as explained in Section 2.1).

Unfortunately, the physical basis on which MEMS accelerometers work makes them also respond to accelerations associated with movement of the module at non-uniform speeds ("Linear Accelerations"). Because of this effect, the "trustworthiness" of the acceleration-based orientation corrections will decay when the MARG module is not static or moving at constant speed.

The basis for using magnetometer readings to support the estimation of MARG orientation is fundamentally the same as for the accelerometer. In this case the constant (in magnitude and orientation) vector field that is hypothesized is the magnetic field of the Earth. We could imagine the local geomagnetic field as represented by arrows of the same length all around us, all of them point towards the North, and forming

the same angle of tilt or "magnetic inclination" with the horizontal plane. This magnetic inclination angle depends on geographic latitude but will be constant within the prospective working space for the glove. Just as with the gravity vector for the accelerometer, this assumed consistency of the geomagnetic field throughout the working space of the system can be leveraged to use instantaneous magnetometer readings to confirm or correct estimates of the orientation of the MARG module (as explained in Section 2.1).

At first, it may seem that the magnetometer readings offer a more robust mechanism to aid in the estimation of MARG orientation, since the magnetometer readings are not distorted by motion of the MARG module. Unfortunately, this information source has a different caveat. In contemporary working environments, where we may want to deploy the instrumented glove to be used for human–computer interaction, there are usually large pieces of ferromagnetic materials (e.g., the iron parts of a desk). Further, contemporary buildings are frequently constituted by metallic structures, which can also alter the geomagnetic fields within them [5]. These objects will have the effect of "bending" the magnetic field lines in their vicinity. For example, a large iron road may provide an "easier" path for magnetic field lines, which will "bend", distorting their original orientation, to run within the ferromagnetic material. Therefore, the magnetic field vector near these magnetic disruptors will have a different orientation, which is a departure from the uniform magnetic field assumption. This reduces the "trustworthiness" of magnetic-based orientation estimates, in the vicinity of ferromagnetic materials.

1.3. Relevant previous work in this area

Over the last several decades there have been numerous approaches proposed for orientation estimation fusing measurements from gyroscope and accelerometer readings (i.e., from IMU modules) first, and later including the additional fusion of magnetometer readings. Nazarahari and Rouhani [3] offer a fairly comprehensive and systematic cataloguing of those efforts, identifying 3 major families of approaches: Vector Observation (VO), Complimentary Filter (CF) and Kalman Filters (KF). Further, these same authors did an experiment to compare 36 Sensor Fusion Algorithms from their survey which could be categorized into 7 major groups: Linear Complementary Filter (LCF), Nonlinear Complementary Filter (NLCF), Linear Kalman Filter (LKF), Extended Kalman Filter (EKF), Complementary Kalman Filter (CKF), Square-root Unscented Kalman Filter (SRUKF), and Square-root Cubature Kalman Filter (SRCKF) [6]. They concluded that the method proposed by Sabatini [7] showed lower errors when time is not a factor, while the methods from Hua et al. [8] or Justa et al. [9] were found to give the best results when the execution time is a factor.

Harindranath [10] created a simulation platform in Matlab that compared another four popular orientation algorithms in a 9-axis MARG unit which are Madgwick Algorithm [11], Mahony Algorithm [12], Extended Kalman Filter and Two Stage KF-Q update. It was found that the Mahony filter performed best in the low level of noise while the Two Stage KF-Q worked well in a higher noise level.

The Kalman filter, envisioned by Dr. Rudolf E. Kalman [13], is one of the most popular methods to estimate the state of a dynamic system for which there is a model and instantaneous observations [14]. In its simplest form, the Kalman Filter obtains an enhanced ("posterior") estimate fusing the results predicted from a model (used as "prior" estimate) with instantaneous measurements through Bayesian Estimation. It is noteworthy that in the Kalman Filter the predicted estimate resulting from the model is "corrected" in the second stage of the process by involvement of the instantaneous measurements. The final state estimate that results has fused the result from the model and the information derived from the instantaneous measurements according to the level of "trustworthiness" of both sources (represented by their covariance matrices). Although the original Kalman filter was developed on the basis of a linear state transformation and the assumption of Gaussian distributions for all the quantities involved, subsequent versions (e.g., "Extended" and "Unscented") of the Kalman filter concept have been adapted for application to non-linear models.

J. L. Marins, et al. [15] studied an extended Kalman filter for quaternion-based orientation estimation of a rigid body motion using MARG sensors, in real-time. Due to the highly nonlinear functions involved in processing data from 3 sensors (gyroscope, accelerometer, and magnetometer), the partial derivatives needed for extended Kalman filtering were very complicated and not applicable for real-time implementation. To be able to use the extended Kalman filter in real-time, Marins needed to apply the Gauss–Newton iteration algorithm in his method. The complexity of using Kalman filtering correction in real-time process is also shown in Peppoloni's study [16] as it highlights the difficulty in correctly setting up and updating the critical Kalman filter parameters.

Some commercial MARG modules used to offer an internally-implemented (Extended) Kalman Filter. For example, the 3-Space sensor Micro USB model from Yost Labs [17], used in our research, provides the Kalman filter as a default filter mode. In it, statistical techniques were used to combine normalized sensor data and reference vector data into a final orientation which can be directly read from the module (This has been done in our research to have a basis for comparison). However, Yost Labs has more recently developed an alternative proprietary filter algorithm called "QGRAD2" [18], which they claim is more efficient and has 3 times faster update rate than their original Kalman filter. Another potential drawback of many Kalman-based approaches is that the levels of "trustworthiness" of the several sources of information (gyroscope-based model, accelerometer- and magnetometer-based measurements) are represented by constant covariance matrices, which is not an exact match with the reality that governs the appropriateness of the accelerometer- or magnetometer-based correction estimates. Some interesting approaches have been proposed to change the "tuning" parameters of the Kalman Filter "on the fly", such as scaling of the measurement covariance matrix, R [19]. Nonetheless, as Mahony et al. pointed out [12], "Traditional linear Kalman filter techniques including EKF techniques have proved extremely difficult to apply robustly to applications with low quality sensors systems".

More recently, some groups have attempted to consider dynamic assessments of the varying levels of "trustworthiness" that must be assigned in making accelerometer- and magnetometer-based orientation corrections. Madgwick [11], indicates that his algorithm "contains 1 (IMU) or 2 (MARG) adjustable parameters defined by observable system characteristics". For the case of an IMU (i.e., no magnetometer) he indicates "The filter gain, β, represents all mean zero gyroscope measurement errors, expressed as the magnitude of a quaternion derivative" However, in his report, Madgwick set these parameters just once for each of his implementations ("The proposed filter's gain β was set to 0.033 for the IMU implementation and 0.041 for the MARG implementation".) These parameters are not, therefore truly dynamic in terms of being re-assigned as frequently as every iteration according to the instantaneous circumstances in which the system is performing.

There have also been studies that have attempted to assess and account for the reduced level of "trustworthiness" associated to the magnetometer-based corrections. Roetenberg et al. [20] showed that the Kalman filter's performance would deteriorate when there is a disturbance of the magnetic field. They attempt the identification of a possible magnetic disturbance on the basis of the magnitude of the total magnetic flux recorded by the magnetometer and the detection of change in the magnetic inclination ("magnetic dip angle") derived from the magnetometer measurements and the current orientation estimate of the MARG module. In 2015, Daponte et al. [21] proposed a new way to estimate the orientation of MARG units with the capability of compensating short-duration magnetic disturbances using a Gradient Descent Algorithm. He continued his research for long-duration disturbances from the magnetometer embedded on a smartphone in

2017 [22] by modeling the disturbances from both hard iron and soft iron. Jin Wu [23] proposed a novel nonlinear optimization approach to address magnetometer disturbances in real-time, using the interior-point method. He proposed that his unique solution could correct the issue efficiently and with a fast response, but this proposed method only deals with soft-iron disturbances that are not very strong.

In recent years, Valenti et al. [24] and our own group have independently proposed an alternative way to execute the "correction" phase of the sensor fusion algorithm for MARG orientation estimation. Based on the work of Shoemake [25], Valenti proposed the use of linear quaternion interpolation (LERP), for small corrections and spherical linear quaternion interpolation (SLERP) only for larger corrections, calculating the correction quaternion (i.e., Δq_{acc}) algebraically and executing the correction in the global (inertial) frame of reference. Based on the report from Dam et al. [26] our group proposed the use of SLERP for all corrections, calculating the quaternion correction (i.e., Δq_A) and executing it in the MARG's body frame, in our initial algorithm, GMV-S [27]. Valenti et al. control the amount of interpolation through a parameter $0 \leq \alpha \leq 1$, which characterizes the cutoff frequency of their complementary filter, as described by De Franceschi and Zardi [28]. Our interpolation control variable was derived from the "confidence" parameter representing how close the MARG is to being static [17]. In their report, Valenti et al. found that their method achieved better results in all three angles (roll, pitch, and yaw) in comparison to the Madgwick filter and the Extended Kalman filter for situations with and without magnetic disturbances.

In 2019, Meyer developed an approach similar to Valenti's but with a more cautious incorporation of the accelerometer measurement [29]. He added layers for checking the accelerometer magnitude error, rate of change of the magnetic field vector and a model of the gyro bias before he fed the data into the estimation correction system. He performed a simulation test with modeled Gaussian noise added to the three sensors. In results from 50 simulation runs, his model was successful in distinguishing slow dynamic maneuvers from biases and could eliminate the problem of pseudo steady-states. However, he indicated that it was too soon to be sure that the filter would be suitable for extended periods of dynamic motion and the filter's robustness to magnetic distortion would need to be investigated more extensively.

As more refined algorithms continue to be developed, the area of application of orientation estimation from MARG signals is expanding. Qiu et al. have recently compiled a comprehensive review of the advances in multisensory information fusion aimed at human activity monitoring and recognition [30]. Their broad overview of the general process by which the information from multiple sensors can be fused efficiently will be very useful in guiding the development of systems where larger numbers of MARG modules must work in coordination. For example, Marta et al. [31] have addressed the requirements that emerge when the orientation estimates from multiple (e.g., 11) MARG modules need to be coordinated to provide simultaneous monitoring of multiple limbs in subjects with their wearable biofeedback suit.

Similarly, the motion capture industry is now beginning to evolve from the exclusive use of vision-based systems, into new products that integrate MARG modules and other types of sensors. As an example, the Xsens MVN line (Awinda Starter, Awinda and MVN Link) offer monitoring of the torso and limbs that can be used "in any setting", as it utilizes 17 MARG-type sensors whose signals are processed by proprietary algorithms. Further, their Xsens Gloves by Manus seek the monitoring of the motion of the fingers with a combination of six MARG-type sensors ("9 DoF IMU") and five 2-degree of freedom "flexible sensors" in each glove.

In any case, the success and prevalence of these emergent multi-MARG systems will be enhanced by the development of innovative approaches to the full utilization and efficient fusion of the signals provide by each of MARG modules, such as the one we propose.

2. Methods and materials

2.1. Description of the GMV-D MARG orientation estimation method

Our method seeks to express a final MARG orientation estimate as a quaternion. The final orientation estimate calculated at each sampling interval (e.g., T = 100 ms), q_{OUT}, conveys the rotation that takes the body coordinate reference on the MARG module to its current orientation, from its initial orientation, when the rotation speed readings from the gyroscope (ωx , ωy and ωz) began to be integrated. The underlying assumption is that the MARG had its body frame initially aligned with the "global" or "inertial" frame to which the MARG orientation is referenced at all times. Due to space limitations, we do not review quaternion arithmetic in this paper. Interested readers can found comprehensive reviews of quaternion arithmetic and interpretation in the books by Kuipers [32] or Hanson [33]. We must, however, emphasize the operation by which a quaternion, q, representing an orientation change, effects that orientation change on a 3-dimensional vector augmented to 4 elements by addition of a 0, (to form a "pure quaternion"). Under those conditions, the rotated vector, v′, is found as:

$$v' = q \otimes v \otimes q^* \tag{1}$$

where q* is the quaternion conjugate of the original quaternion q, and ⊗ represents quaternion multiplication. Furthermore, while Eq. (1) would rotate vector v to v′ within the same frame of reference, the following manipulation amounts to re-defining in v′ the same vector v, but know in a second (MARG body) reference frame which has been rotated according to q from a first (inertial, global) frame of reference:

$$v' = q^* \otimes v \otimes q \tag{2}$$

Our algorithm will be executed, iteratively, every sampling time. Every execution presumes that there are available current tri-axial readings from the gyroscope, the accelerometer and the magnetometer within the MARG module, as well as tri-axial position coordinates from the IR-camera system. In addition, we also read the "confidence" parameter generated by the Yost Labs 3-Space MARG module. For other devices, an equivalent parameter can be calculated from accelerometer and gyroscope readings. With these values, the GMV-D algorithm proceeds through the following phases:

Phase I: Generation of an initial estimate by integration of the gyroscope signals- Similar to the Kalman Filter, our approach generates an initial orientation estimate by "dead reckoning", i.e., the successive integration of orientation changes approximated on the bases of the angular speeds read from the gyroscope in the last sampling interval. In quaternion form, this initial orientation estimate, q_G, is found as:

$$\dot{q} = \frac{1}{2}\hat{q}_0 \otimes \omega_B \tag{3}$$

$$q_G = e^{((\Delta t)\dot{q} \otimes \hat{q}_0^*) \otimes \hat{q}_0} \tag{4}$$

where ω_B represents the latest gyroscope readings after a process of offset (bias) removal which involves the subtraction of the current bias offset estimate from the raw gyroscope readings. In Eq. (4), $\hat{q}_0$, is the MARG orientation estimate from the previous iteration (at the previous sampling instant). For the very first execution of Eq. (4), $\hat{q}_0$ is given as initial value the quaternion that represents "no rotation", which would be $[0, 0, 0, 1]^T$ if the quaternions are being represented with their "real" component in the last position. Prior to the first execution of the algorithm, while the MARG is static, multiple readings of tri-axial acceleration are taken and averaged to be stored as a vector of initial acceleration, A_{int}. Similarly, an initial magnetic vector, M_{int}, is recorded.

Phase II-A: Definition of the predicted acceleration vector (in body frame)- As Markley and Mortari remarked in their 2000 paper [4] "It

is well known that [at least] two vector [observations] are sufficient to determine the attitude [of a rigid body]". Therefore, attitude cannot be fully characterized by observation of the acceleration vector alone. Instead, our approach seeks to *supplement* the initial orientation estimation from gyroscope signals (q_G) with information obtained from the observation of acceleration, in Phases II-A, and III-A, resulting in a quaternion, q_{GA} that has been (fully) corrected using acceleration measurements.

The gravity vector can reasonably be expected to have the same orientation (i.e., vertical, pointing to the floor) throughout the operation of the system. Thus, the 3 accelerometer readings that the gravity alone should be producing in the MARG at any iteration can be estimated by applying the dead reckoning estimate of the MARG body orientation, q_G, to rotate the initial acceleration vector, A_{int}, to the current orientation of the MARG body. This is the "predicted acceleration reading", $\vec{a}(q_G)$ in the body frame, for this iteration:

$$\vec{a}(q_G) = q_G^* \otimes A_{int} \otimes q_G \tag{5}$$

Phase II-M: Definition of the predicted magnetic vector (in body frame)- Simultaneously, our approach also seeks to *supplement* the initial orientation estimation from gyroscope signals (q_G) with information obtained from observation of the geomagnetic field, in Phases II-M, and III-M, resulting in a quaternion, q_{GM} that has been (fully) corrected using magnetometer measurements.

In the same way described for the definition of the predicted acceleration, a "predicted magnetic reading", $\vec{m}(q_G)$, is found by rotating the initial magnetic vector, M_{int}, using our dead-reckoning estimation of the orientation of the MARG, q_G:

$$\vec{m}(q_G) = q_G^* \otimes M_{int} \otimes q_G \tag{6}$$

As their notations indicate, both of these predictions depend on q_G, and will be inaccurate if the initial (dead reckoning) estimate of the current orientation of the MARG, q_G, contains error, e.g., if, the debiased ω_B gyroscope measurements used in calculating q_G still contain some amount of offset.

Phase III-A: Computation of an accelerometer-based correction in quaternion form (Δq_A)- Adopting (without justification, at this point) the assumption that in a given iteration the MARG module is static or moving without change of speed in all 3 body axes, the predicted acceleration reading, $\vec{a}(q_G)$, would match the instantaneous current reading of the accelerometer, a_0, reacting to gravity. However, in reality, even if the MARG is static, $\vec{a}(q_G)$ will likely have a different direction than a_0, because the dead reckoning estimate, q_G, used to obtain $\vec{a}(q_G)$ may still be impacted by residual drift error from the gyroscope bias. In this stage we make the assumptions:

(1) The current accelerometer readings, a_0, are only reacting to the acceleration of gravity. (We will address how we manage the likely deviation from this assumption in the following paragraphs.)

(2) The initial, dead reckoning MARG orientation estimate, q_G, may contain residual drift error and must be corrected, so as to prevent that drift error from continuing to grow.

In this context we now seek to find the additional "correction" rotation that must be used to "supplement" q_G, in such a way that the newly defined "accelerometer corrected orientation", (symbolized q_{GA},) would rotate A_{int} to match a_0. The "compounding" of 2 rotations represented by quaternions is easily accomplished multiplying the quaternion that represent the individual rotations. So, the accelerometer-corrected orientation quaternion, q_{GA}, is found as:

$$q_{GA} = q_G \otimes \Delta q_A \tag{7}$$

where Δq_A is the quaternion representing that "additional" rotation that would result in q_{GA} being able to rotate A_{int} to match a_0.

The 3-element "imaginary part", $\vec{q}_{Av}$, and the "scalar part", q_{Aw}, of the accelerometer correction quaternion, Δq_A, are computed separately (following the reasoning in the Appendix), and assembled together, with the $\mathcal{H}$ operator:

$$\Delta q_A = \mathcal{H}(\vec{q}_{Av}, q_{Aw}) \tag{8}$$

where

$$\vec{q}_{Av} = \vec{a}_0 \times \vec{a}(q_G) \tag{9}$$

$$q_{Aw} = \|\vec{a}_0\|\|\vec{a}(q_G)\| + \vec{a}_0 \cdot \vec{a}(q_G) \tag{10}$$

Phase III-M: Computation of a magnetometer-based correction in quaternion form (Δq_M)- In the same fashion as for the definition of the accelerometer correction quaternion, we will find a "magnetometer correction quaternion", Δq_M. For this, we will make these assumptions:

(1) The current magnetometer readings, m_0, reflect the geomagnetic field at the current location of the MARG module and we assume that the geomagnetic field at this location has the same direction as the initial magnetic field recorded. (We will address how we manage the likely deviation from this assumption in the following paragraphs.)

(2) The initial, dead reckoning MARG orientation estimate, q_G, may contain residual drift error and must be corrected, so as to prevent that drift error from continuing to grow.

In this context, and proceeding as we did for the accelerometer correction, we will now generate a magnetometer-corrected orientation quaternion, q_{GM}, as:

$$q_{GM} = q_G \otimes \Delta q_M \tag{11}$$

where, proceeding as we did for the accelerometer correction:

$$\Delta q_M = \mathcal{H}(\vec{q}_{Mv}, q_{Mw}) \tag{12}$$

where

$$\vec{q}_{Mv} = \vec{m}_0 \times \vec{m}(q_G) \tag{13}$$

$$q_{Mw} = \|\vec{m}_0\|\|\vec{m}(q_G)\| + \vec{m}_0 \cdot \vec{m}(q_G) \tag{14}$$

After completion of the previously described phases, the system will have, at each iteration, three quaternions that estimate the orientation of the body of the MARG with respect to the inertial, global frame: The initial estimate, provided by sequential integration of the gyroscope signal, q_G; an estimate that has been fully corrected on the basis of instantaneous accelerometer measurements, q_{GA}, and an estimate that has been fully corrected on the basis of instantaneous magnetometer measurements, q_{GM}. However, each of these 3 orientation estimates would only be accurate if the circumstances shown in Table 1 are met.

The goal of our algorithm is to fuse these 3 prospective orientation estimates minimizing the influence of the corrected estimates when their conditions for accuracy cannot be considered properly met. For this purpose, we calculate the 2 parameters shown in the last column of Table 1. These numerical parameters (real values between 0 and 1) are meant to encode to what degree the accuracy requirements for q_{GA} and q_{GM} are met and, therefore, how trustworthy these corrections are.

PHASE IV-A: Computation of α - Prior to being used to determine the value of the control parameter α, the average of recent stillness ("confidence") values read from the MARG module are processed by a first-order Gamma filter to smoothen the signal. The Gamma filter uses a weight parameter (W), which ranges from 0 to 1, to control the filtering characteristics of the low pass filter it implements on the signal. (We selected $W_\alpha = 0.25$.) The first-order Gamma filter has the difference equation derived in Eqs. (15) to (18).

$$H(z) = \frac{Y(z)}{X(z)} = \frac{W}{z - (1 - W)} \tag{15}$$

$$Y(z) = (W)z^{-1}X(z) + (1 - W)z^{-1}Y(z) \tag{16}$$

$$y[n] = (W)x[n - 1] + (1 - W)y[n - 1] \tag{17}$$

Table 1
Three prospective MARG orientation estimates.

Orientation estimate	Corrected or uncorrected	Obtained by	Requirement for accuracy	Parameter encoding requirement compliance
q_G	Uncorrected	Sequential integration of gyroscope signals	Drift has been eliminated by removing gyroscope biases completely.	–
q_{GA}	Fully corrected by accelerometer information	Forcing the estimate to rotate A_{int} to the instantaneous a_0	MARG is static, a_0 represents only gravity.	$0 \le \alpha \le 1$
q_{GM}	Fully corrected by magnetometer information	Forcing the estimate to rotate M_{int} to the instantaneous m_0	Local geomagnetic field, measured in m_0, is the same as in the initial location.	$0 \le \mu \le 1$

$$\alpha_g[n] = W_\alpha(Stillness[n-1])^2 + (1 - W_\alpha)\alpha_g[n-1] \tag{18}$$

Then a linear equation, with slope m_α, was applied to accelerate the drop of the α parameter when the sensor begins departing from a static status. The final α parameter is calculated through Eqs. (19) and (20).

$$\alpha' = m_\alpha \alpha_g + (1 - m_\alpha) \tag{19}$$

$$\alpha = \frac{\alpha' + |\alpha'|}{2} \tag{20}$$

PHASE IV-M: Computation of μ - According to (C1b) from the operational constraints we have determined for our system (Section 1.1), we expect that local distortions of the geomagnetic field will occur at positions that are fixed or slowly-varying in the working space of the system. Therefore, we attach different values of μ to different regions in the working space of the system. As we do not know the actual value of μ for any region when the system starts operating, the value of μ for all regions is initialized to 0. To define this Magnetic Correction Trustworthiness parameter (μ), the current position data from the OptiTrack system is used to determine the location of the MARG module. The working space of the system is divided in small 3-D cubes or "voxels" and the voxel in which the MARG module is currently contained is determined using Eq. (21) in the 3 coordinate axes:

$$VoxelIndex = floor(\frac{CurrentCoordinate}{VoxelSize}) + 1 \tag{21}$$

To be able to update the value of μ of the current voxel to a useful one, the current value of α is compared against a threshold, α_{TH}. If $\alpha \ge \alpha_{TH}$, we can expect that the correction suggested by the accelerometer, here identified as $\hat{q}_{Gpost} = \hat{q}_{GA}$, is correct. This will provide an opportunity to update the value of μ for the current voxel. For this purpose, we will assess the difference between the magnetic field direction captured by the magnetometer readings, m_0 and the one calculated by rotating the initial magnetic field vector, M_{int}, with the recently computed $\hat{q}_{Gpost}$, which we trust to be correct. To do this, we compute the angle γ, whose cosine, ranging from −1 to 1, represents the level of alignment between these 2 directions, as illustrated in Table 2. The parameter μ is computed from cosine of γ by rescaling and application of a linear equation to severely penalize departures from perfect agreement (which would yield $\mu = 1$):

$$\vec{\mu}\left(\hat{q}_{Gpost}\right) = \hat{q}^*_{Gpost} \bigotimes M_{int} \bigotimes \hat{q}_{Gpost} \tag{22}$$

$$cos(\gamma) = \frac{\vec{m}_0 \vec{\mu}\left(\hat{q}_{Gpost}\right)}{|\vec{m}_0|\left|\vec{\mu}\left(\hat{q}_{Gpost}\right)\right|} \tag{23}$$

$$\mu' = -m_m(acos(cos(\gamma))) + 1 \tag{24}$$

$$\mu = \frac{(1 + \mu')}{2} \tag{25}$$

$(if\ \mu < 0,\ \mu is\ overwritten\ as\ 0)$

It is expected that, as the user moves his/her hand through the working space of the system, the initial $\mu = 0$ values assigned at initialization will be updated by μ values that really reflect the magnetic trustworthiness of the regions visited by the module. This will enable the effective consideration of magnetometer-based corrections in more instances, while simultaneously preventing magnetometer corrections from introducing large errors where the magnetic field is distorted.

PHASE V: Definition of the final orientation estimate for the current iteration by double SLERP interpolation- Previously, an initial Gravity and Magnetic-Vector Compensation, involving a single SLERP interpolation (GMV-S) approach was introduced by O-larnnithipong [27]. That algorithm implements a correction of q_G using signals from both accelerometer and magnetometer, but under exclusive control of a single parameter, α, and does not attempt to detect magnetically distorted regions in the working space of the sensor. An accelerometer-based corrected orientation $\hat{q}_{GA}$ is calculated and, similarly, a magnetometer-based corrected orientation, $\hat{q}_{GM}$ is also defined. Then, GMV-S uses a single SLERP interpolation, from $\hat{q}_{GM}$ to $\hat{q}_{GA}$, to define the final orientation quaternion, solely under control of α, bringing the final result closer to $\hat{q}_{GA}$ when α is closer to 1.

The SLERP interpolation between the rotation indicated by a quaternion q_0 and a quaternion q_1, controlled by the parameter $0 \le h \le 1$, is calculated as [25] :

$$SLERP(q_0, q_1, h) = \frac{q_0\ sin((1-h)\Omega) + q_1 sin(h\Omega)}{sin(\Omega)} \tag{26}$$

where,

$$\Omega = cos^{-1}(\hat{q}_0 \cdot \hat{q}_1) \tag{27}$$

So, GMV-S defined the final orientation estimate for the iteration, $\hat{q}_{OUT}$, as:

$$\hat{q}_{OUT} = SLERP(\hat{q}_{GM}, \hat{q}_{GA}, \alpha) \tag{28}$$

This followed the logic that, if the MARG module is very close to a static condition, the accelerometer-based correction is trustworthy.

However, if the sensor operates in a magnetically distorted region, when simultaneously α is low, the previous method may still give $\hat{q}_{GM}$ a large weight in the definition of the final corrected orientation estimate. This could lead to orientation estimate errors, in those particular circumstances. Our new method prevents those performance shortcomings by assessing the magnetic trustworthiness, encoded in μ, and using this parameter to constrain the magnetometer-based correction in the quaternion interpolation also.

As the computer user proceeds to operate the system, the processing of the data from the MARG module will fall approximately into one of 4 broad cases at every sampling time, which are summarized in Table 3. At every sampling instant, the position of the sensor will be retrieved from the OptiTrack system and, with this and the readings from the MARG module, the control parameters α and μ will be obtained and used to determine the contribution of the accelerometer-based correction and the magnetometer-based correction to the final orientation estimate.

The final orientation estimate will be calculated from 2 preliminary results, $\hat{q}_{SA}$ and $\hat{q}_{SM}$, which represent "scaled" interpolated accelerometer-based and magnetometer-based corrections to $\hat{q}_G$, through the corresponding SLERP operations described in Eqs. (29) and (30) :

$$\hat{q}_{SA} = SLERP(\hat{q}_G, \hat{q}_{GA}, \alpha) \tag{29}$$

Table 2
Magnetic Correction Trustworthiness (μ) values for different angles between the current geomagnetic vector ($\vec{m}_0$) and the vector derived from the accelerometer corrected quaternion $\vec{\mu}(q_{Gpost})$.

Vectors	γ	$\cos(\gamma)$	μ
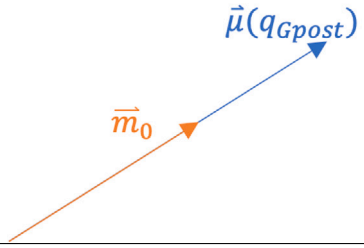	$\sim 0°$	1	1
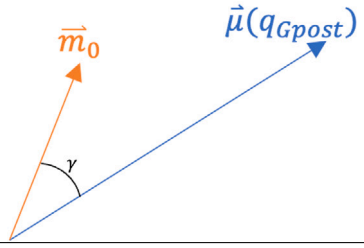	$0° \leq \gamma \leq 90°$	$0 \leq cos(\gamma) \leq 1$	$0.5 \leq \mu \leq 1$
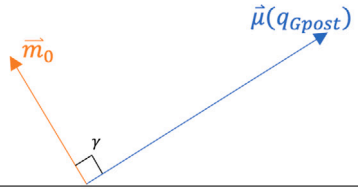	$\gamma = 90°$	0	0.5
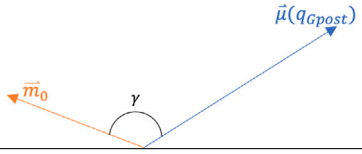	$90° \leq \gamma \leq 180°$	$-1 \leq cos(\gamma) \leq 0$	$0 \leq \mu \leq 0.5$
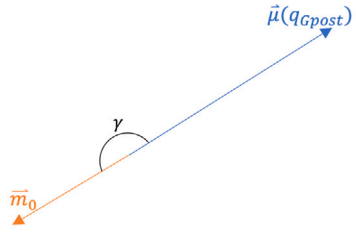	$\gamma = 180°$	-1	0

$$\hat{q}_{SM} = SLERP(\hat{q}_G, \hat{q}_{GM}, \mu) \tag{30}$$

It must be noticed that, if α is low, $\hat{q}_{SA}$ will not be much different from $\hat{q}_G$. Similarly, if μ is low, $\hat{q}_{SM}$ will not be much different from $\hat{q}_G$. The final orientation estimate will then be obtained from a second SLERP operation on both of the preliminary results, and controlled by α:

$$\hat{q}_{out} = SLERP(\hat{q}_{SM}, \hat{q}_{SA}, \alpha) \tag{31}$$

The overall effects expected from the two-tiered SLERP corrections are presented in Table 3, where its possible to verify that the final orientation estimate, $\hat{q}_{out}$, will largely disregard correction components for which the trustworthiness parameters are low.

Table 3
Definition of the final orientation in 4 cases of μ and α values.

CASE	Control		Procedure $\hat{q}_{out}$ is final orientation estimated		
	$\mu \simeq$	$\alpha \simeq$			
0	0	0	$\hat{q}_{SA} \approx \hat{q}_G$;	$\hat{q}_{SM} \approx \hat{q}_G$;	$\Rightarrow \hat{q}_{out} \approx \hat{q}_G$
1	0	1	$\hat{q}_{SA} \approx \hat{q}_{GA}$;	$\hat{q}_{SM} \approx \hat{q}_G$;	$\Rightarrow \hat{q}_{out} \approx \hat{q}_{GA}$
2	1	0	$\hat{q}_{SA} \approx \hat{q}_G$;	$\hat{q}_{SM} \approx \hat{q}_{GM}$;	$\Rightarrow \hat{q}_{out} \approx \hat{q}_{GM}$
3	1	1	$\hat{q}_{SA} \approx \hat{q}_{GA}$;	$\hat{q}_{SM} \approx \hat{q}_{GM}$;	$\Rightarrow \hat{q}_{out} \approx \hat{q}_{GA}$

2.2. Block diagram for the Gravity and Magnetic North Vector orientation correction with Double SLERP (GMV-D) algorithm

Fig. 1 displays the block diagram representing the complete operation of the GMV-D algorithm. It should be emphasized that the

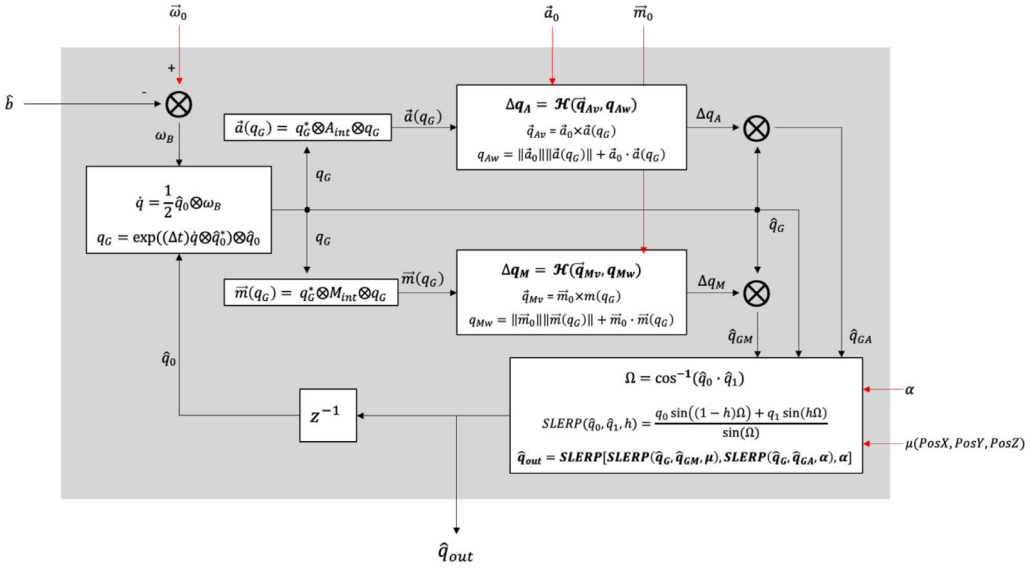

Fig. 1. Block diagram of the orientation correction algorithm using the gravity vector and magnetic North vector with double SLERP (GMV-D).

final MARG orientation estimate, $\hat{q}_{OUT}$, is offered as final result of the iteration and it is also fed back as the "previous orientation", $\hat{q}_0$, that will be used to accumulate the new bias-compensated gyroscope readings, ω_B, in the next iteration (indicated in the block diagram through the unit delay, z^{-1}, block).

2.3. Evaluation procedure

While MARG modules will prospectively be attached to the fingers and dorsal surface (opposite from the palm) of a glove, in our testing protocol the module was attached to a small wooden block, so that our subjects could ensure orthogonal orientations by simply resting a specific side of the block, flushed against a leveled horizontal surface.

The experiment space was set up away from ferromagnetic objects, using wooden supports for the flat surface where the "home position" of the MARG module was defined for the experiment. Similarly, a wooden stool was used to support an iron bar (0.5 × 3.8 × 37.5 cm), at the same height as the "home position" for the MARG, about 60 cm. away from it. Therefore, only the space near the iron bar was expected to be magnetically distorted. The OptiTrack V120: Trio module, containing 3 IR video cameras in a 58.4 cm enclosure, was placed in front of the experimental area, so that position readings could be obtained from it throughout the experiment. The experimental subject was instructed to lift the module from the "home position" and perform a number of rotational movements in the non-magnetically distorted area. Then the subject would translate the module to the area above the iron bar (magnetically distorted area) and repeat *the same sequence* of rotational movements. Finally, the subject would translate the module back to the "home position" and the experimental trial ended.

In order to explore the potential differences in results that could stem from different movement speeds and trajectories, within the range of human motion, we recruited 30 (22 males, 8 females, all right-handed) volunteer subjects, who followed the protocol described above. Their ages ranged from 18 to 60 years old. None of the subjects reported any motion impairment which could affect the performance of the evaluation task.

The Yost Labs 3-Space MARG module was connected to a processing PC with a USB cable. The OptiTrack V120: Trio module was also connected to the same PC, via USB. A C♯ program running under Unity showed the subject (graphically) what to do and collected position data and 3-axial gyroscope, accelerometer, and magnetometer data from the OptiTrack and Yost Labs sensors, respectively. This same program, additionally, computed the initial estimation of orientation by accumulation of gyroscopic data ($\hat{q}_G$) and applied, in real time, the complete proposed GMV-D correction process shown in the block diagram of Fig. 1. For the purpose of comparison, the program also computed the correction using our previous algorithm, GMV-S, in which a single SLERP operation is applied to perform interpolation from $\hat{q}_{GM}$ to $\hat{q}_{GA}$ under the control of α, only. That previous algorithm does not calculate the μ parameter on the basis of position. (That previous, GMV-S, algorithm is fully explained in [27]). The evaluation setup is depicted in Figs. 2 and 3.

3. Results

3.1. Comparison of quaternion components

To verify the results of the proposed algorithm, the corrected orientation was expressed as a quaternion ($\hat{q}_{OUT}$ in Fig. 1) for the GMV-D method and compared with three other methods: Fixed bias, Kalman filtering, and GMV-S. The fixed bias method only compensates the gyroscope bias once, at system initialization, and does not correct the orientation estimate. The Kalman filter method is implemented internally by the MARG module used. Three of the numbers contained in a quaternion (in our case, $\hat{q}_x$, $\hat{q}_y$ and $\hat{q}_z$) represent an axis vector in 3-dimensional space, and the 4th component ($\hat{q}_w$ in our case), indicates the amount of rotation to be performed [5]. Therefore, we display the 4 components of the output orientation quaternion through the duration of a representative experimental trial to analyze the results (Fig. 4). The panels in Fig. 4 show the evolution of the 4 quaternion components from the 4 methods, for the complete duration of the experimental trial (The horizontal axes are labeled in samples, where the sampling interval was 100 ms). The first half of the record (left of the vertical green dividing line) corresponds to the rotations that took place in the area that was not magnetically distorted. The second part of the record (to the right of the green line) represents the same sequence of rotations performed in the magnetically distorted area. The 4 quaternion components in the top panel ("fixed bias") display drift that grows gradually throughout the trial, with and without magnetic distortion. All other methods ("Kalman filter", "GMV-S", and "GMV-D") performed very similarly when magnetic distortion was not present. However, both the Kalman filter and GMV-S show erroneous results in the magnetically distorted area. The bottom panel of Fig. 4 shows the corresponding output quaternion components obtained from our proposed GMV-D algorithm, which displays performance that was much less deteriorated when the rotations took place in the magnetically distorted area.

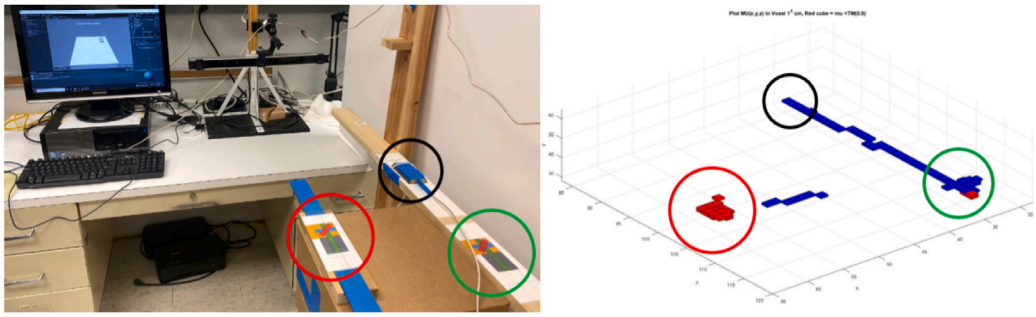

Fig. 2. Experimental setup. In the photograph (left), circles indicate: "home position" (black), non-magnetically distorted area (green) and magnetically-distorted area (red). The same circles identify these areas in the 3-D plot, where previously visited voxels were colored red if $\mu < 0.9$, and blue otherwise. (For interpretation of the references to color in this figure legend, the reader is referred to the web version of this article.)

Fig. 3. Human subject performing the experimental protocol.

3.2. Orientation visualizations

The black numerals in Fig. 4 (1 to 10) help identify short segments during the trial when the subject was instructed to sustain specific hand orientations or "poses". The corresponding instructed poses are visualized in 3-D, in Figs. 5 and 6, under "Sequence Reference" (leftmost column). In each pose, the 4 visualizations that are shown to the right of the instructed pose are defined (in Unity) by the quaternion results obtained from "Fixed bias", "Kalman filter", "GMV-S", and "GMV-D", from left to right, respectively. This additional form of visualization shows that the orientations obtained from GMV-D were much closer to the orientations that the subject was instructed to temporarily maintain, particularly when the rotations took place in the magnetically distorted zone (Poses 6 through 10). Figs. 4, 5 and 6 confirm that the added processing integrated with GMV-D has made it more resilient to the potential distortion of the magnetic field that may exist in some regions of the working space for the MARG.

3.3. Additional quaternion comparisons

Our initial interest was to compare GMV-D against our previous method (GMV-S), to confirm the expected improvement, and against a classical method that everyone could relate to (Kalman Filtering implemented within the MARG module by the manufacturer). However, it was also interesting to compare GMV-D to two of the other MARG orientation algorithms that Harindranath et al. [10] included in their 4-way comparison. These are the algorithms developed by S. O. H. Madgwick [11] and R. Mahony et al. [12]. In order to implement the comparison, data from the same representative experimental trial used to generate Figs. 4, 5 and 6 were processed by the Matlab implementations of the Madgwick and Mahoney algorithms authored by Madgwick and made available at https://x-io.co.uk/open-source-imu-and-ahrs-algorithms/. Our data was up-sampled to a sampling rate of 256 Hz, to match the rate expected by the implementations, which were not modified in any way (The parameters assigned were the same as in the examples accompanying the implementations: Beta = 0.1 for Madgwick's and Kp = 0.5 for Mahony's). Fig. 7 shows the evolution of the 4 quaternion components obtained from GMV-D and the other 2 methods.

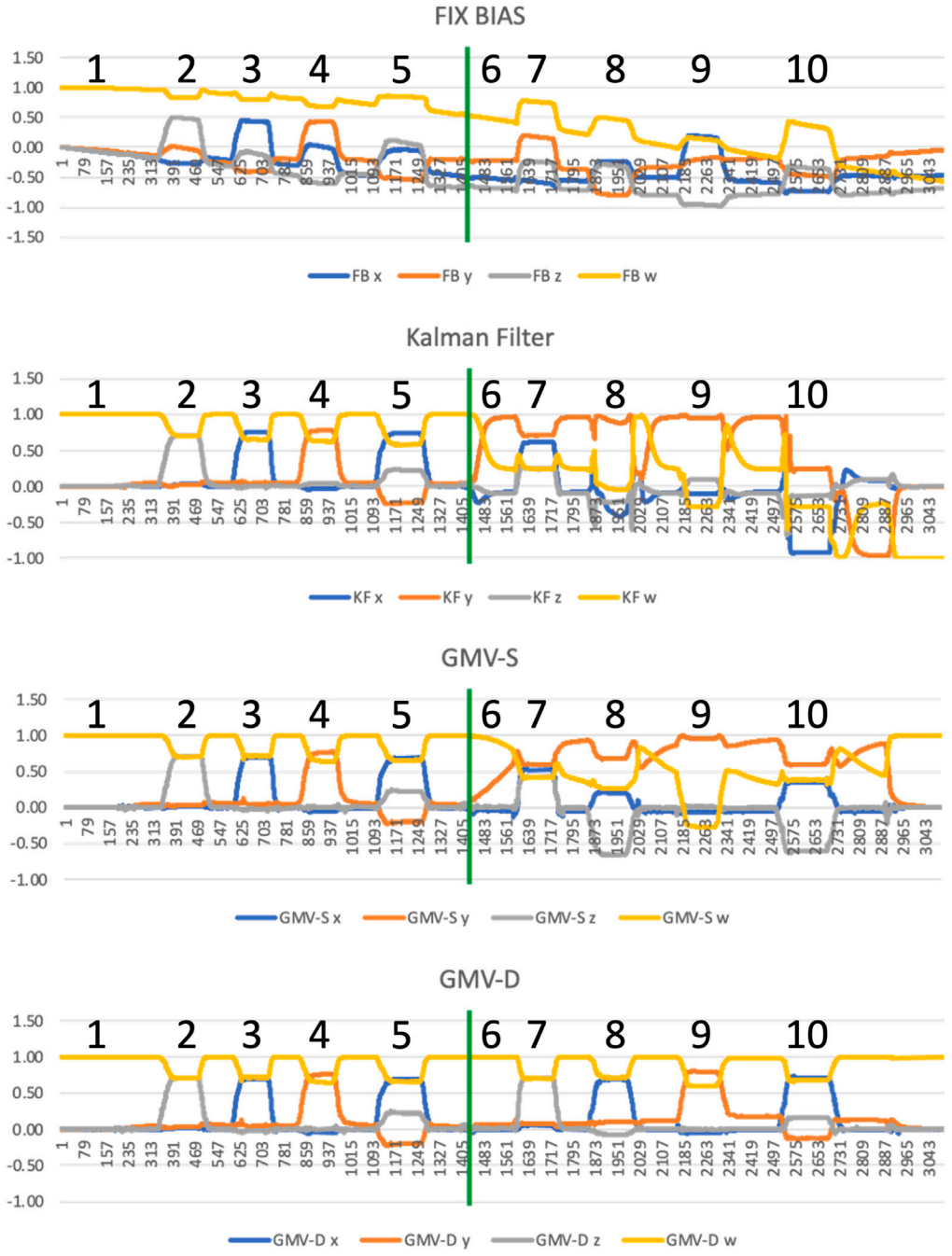

Fig. 4. Quaternion components (4) from each one of the orientation estimation methods, plotted throughout 1 complete (typical) experimental trial. The Fixed Bias method displays drift from the beginning of the session. KF, GMV-S and GMV-D generate similar results in the non-magnetically distorted area, but KF and GMV-S display significantly deteriorated performance in the magnetically distorted area (after the vertical green dividing line). (For interpretation of the references to color in this figure legend, the reader is referred to the web version of this article.)

During the interval when the rotations were performed in the magnetically distorted area (to the right of the green dividing line), GMV-D displays an evolution of the quaternion components that is a close replica of the evolution during the first part of the record, as expected. Madgwick's algorithm displays a nearly identical evolution of quaternion components to GMV-D while the rotations were performed in the area that was not magnetically distorted (to the left of the green dividing line), but shows heavily distorted evolutions of the quaternion components during the part of the record that corresponds to the magnetically distorted area. Mahony's algorithm follows a similar pattern as GMV-D during the first part of the record, except that immediately after each rotation the quaternion components seem to "overshoot" and then *slowly settle down*. It may be that GMV-D avoids this shortcoming because in it the "strength" of the correction in any iteration is not bound by a pre-defined tuning parameter. Instead, in any given iteration, GMV-D can apply even a "full correction" (e.g., assign $q_{SA} \approx q_{GA}$) for as long as the correction meets its corresponding pe-condition (e.g., $\alpha \approx 1$) at that particular time. This makes GMV-D less prone to requiring extended "settling times", like those seen in the output from Mahony's algorithm. This "decaying" effect in Mahony's output is further accentuated in the second part of the record, where, in addition, two of the quaternion components wander away from the levels they took during the same rotations in the area which was not magnetically

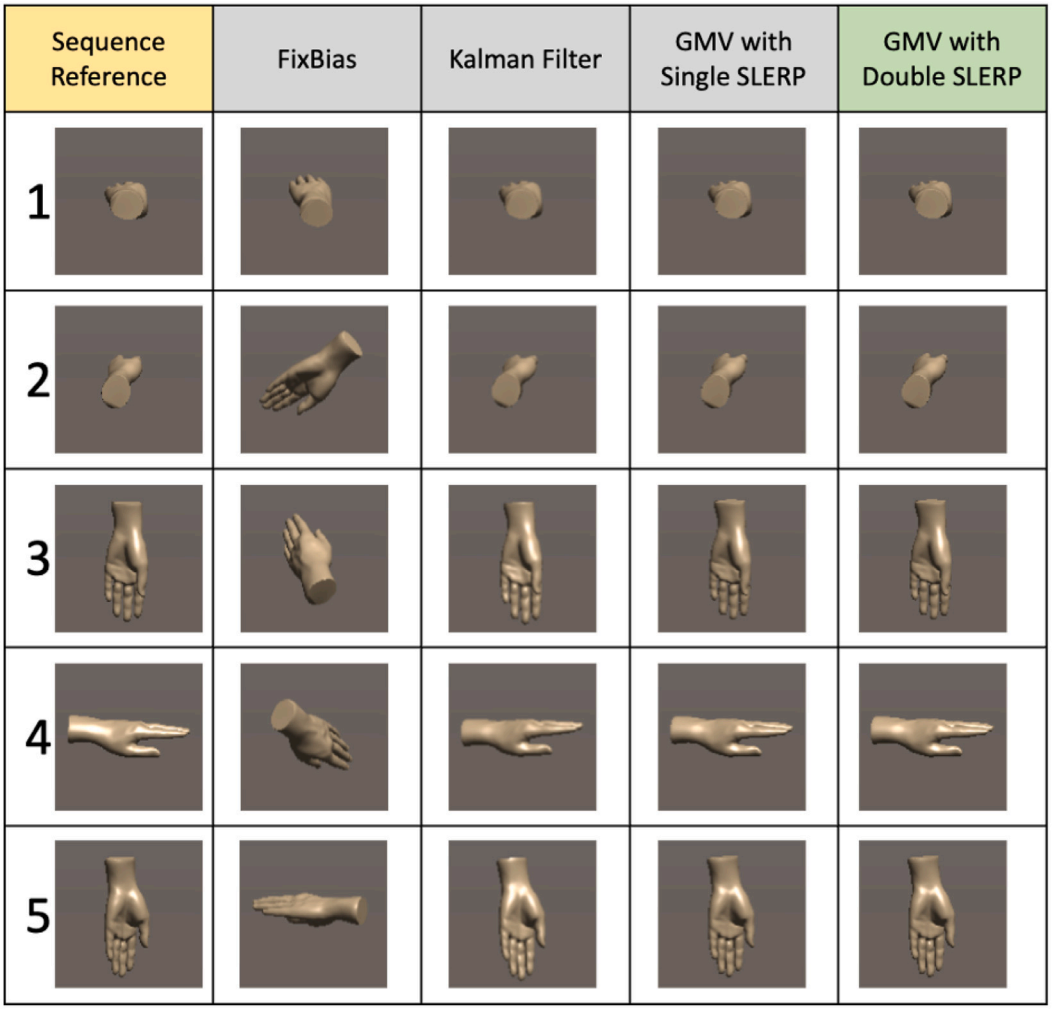

Fig. 5. Renderings of a 3-D hand model rotated according to the quaternion components shown in Fig. 4, specifically at the time instants (poses) identified in Fig. 4 and in the left margin of this figure. Poses 1–5 took place in the non-magnetically distorted area, and the results from KF, GMV-S and GMV-D are similar.

disturbed. Overall, these plots confirm that GMV-D has an improved level of resilience to the presence of magnetic distortions.

3.4. Multi-subject evaluation

As the target application of our MARG orientation algorithm is the tracking of the hand of a computer user, we sought to evaluate the performance of GMV-D, and compare it to the performance of GMV-S and the Kalman Filter built into the MARG module in that particular context. Therefore, 30 different human subjects were asked to manipulate the small wooden block that had the MARG module attached to it. Each subject completed the same trial, as described above, in which the MARG module was first held at 9 poses (first Pose 1, then Poses 2, 3, 4 and 5, with a return to Pose 1 after each) in the magnetically undisturbed area. Then, the subject translated (without rotation) the MARG module to the magnetically distorted area and held the module in the same 9 poses as before (those are now identified as Pose 6 and then 7, 8, 9 and 10 with returns to 6). Since the Fixed bias method was seen to perform very poorly (Figs. 4, 5 and 6), the analysis of multi-subject data concentrated only on 3 algorithms: Kalman Filter (KF), GMV-S, and GMV-D. For each of the 30 subjects, the quaternion result from each one of the 3 algorithms, at each of the 18 poses, was converted to Euler Angles (Phi, Theta and Psi, which represent the value of the angles rotated about the x, y and z axes). Since the "ideal" values of those Euler Angles (as instructed to the subjects) were known, the computations were performed on the angle errors. That is, we studied the deviation of the corresponding Euler Angles reported by the 3 methods from "reference angles" defined by the instructions given to the subjects. As a result, the complete experiment yielded a total of 1620 rows of angular error data (30 subjects × 18 orientations × 3 algorithms) for each of the 3 Euler Angles.

3.5. Root mean square error results

A metric that can be used to compare the performance of the 3 algorithms studied is the square root of the mean of the squared angular errors incurred by the 30 subjects, at any particular pose, i.e., the Root Mean Squared Error (RMSE). Of course, since the three Euler Angles were recorded, the analysis must be performed for each of the Euler Angles: Phi, Theta and Psi. Fig. 8 shows the results of those analyses in three panels. The top panel shows the RMSE for the Phi angles. The horizontal numbers represent the sequence of 18 poses, with the first 9 corresponding to the magnetically undisturbed area and the last 9 corresponding to the magnetically distorted area. The three traces are identified by line color and style in the legend inset within the panel. The middle panel represents the RMSE for the Theta angles, and the bottom panel represents RMSE for the Psi angles, in the same way.

Overall, it can be noticed that in the first 9 poses of the sequence (magnetically undisturbed area), all three algorithms display similar RMSE levels. However, for the last 9 poses (magnetically distorted

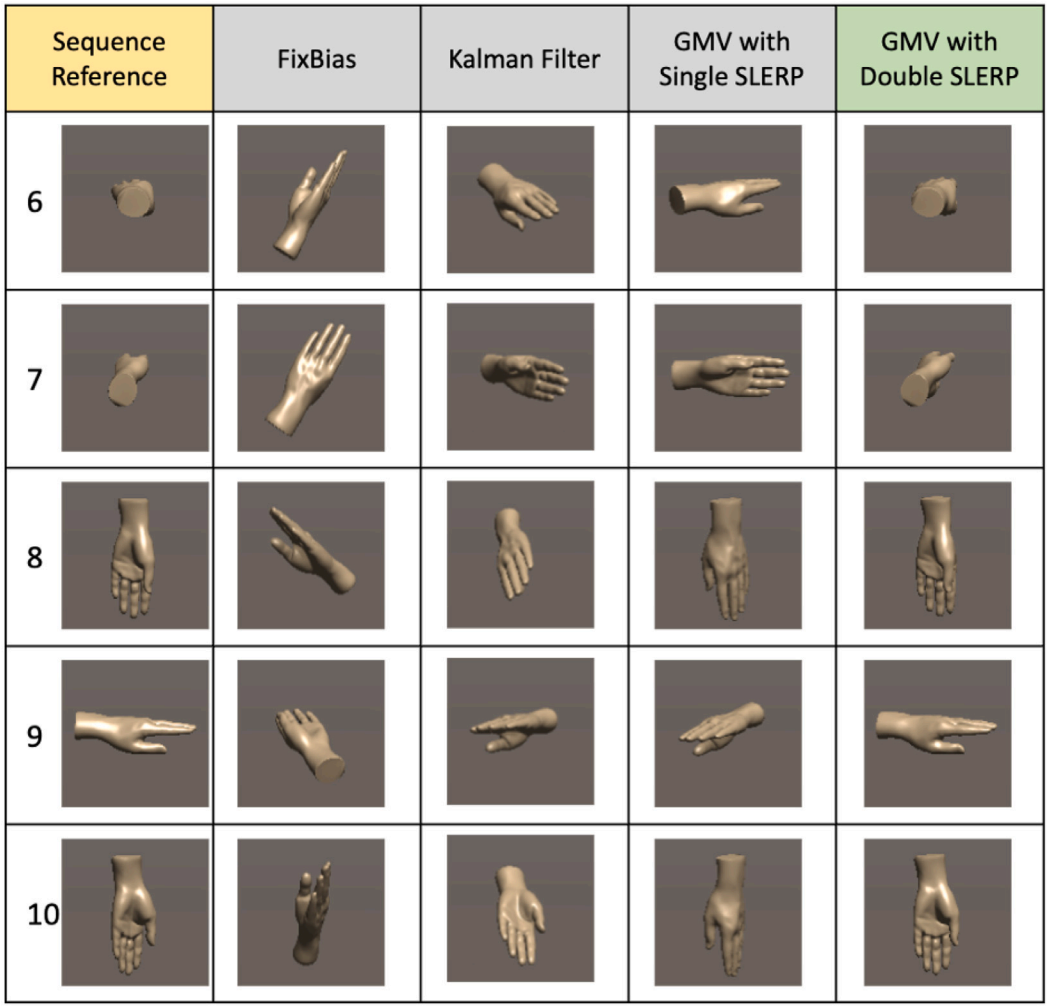

Fig. 6. Renderings of a 3-D hand model rotated according to the quaternion components shown in Fig. 4, specifically at the time instants (poses) identified in Fig. 4 and in the left margin of this figure. Poses 6–10 took place in the magnetically distorted area, and only the new GMV-D method (5th column) yielded orientations that are similar to the reference orientations, shown in the 1st column.

Table 4
18-pose average RMSE values of the 3 algorithms for the 3 Euler Angles.

Euler angle	GMV-D	GMV-S	KF
Phi	2.2359	5.7913	12.6590
Theta	9.8322	44.6486	59.8270
Psi	4.9346	20.1550	20.5489

area), the RMSE levels produced by GMV-D are considerably lower than those produced by GMV-S and KF.

Table 4 shows the RMSE averages (over the 18 poses) for the three algorithms, and summarizes the observations from the graph. That is, it confirms that GMV-D provides orientation estimates that are less susceptible to the impact of magnetic disturbances in the environment.

3.6. Statistical assessment

While the RMSE averages from GMV-D were much lower than those from GMV-S and KF, we sought to perform a more comprehensive statistical assessment which would take into account not only the mean values but also the dispersion of values about the means to determine if there were statistically significant differences in the Phi, Theta and Psi errors that were found when different algorithms were applied to estimate the orientation of the MARG module. The Euler Angle error data were tested and found not to be normally distributed and heterogeneous in variances [34]. Therefore, we utilized the Kruskal–Wallis rank-based nonparametric test, which is used to determine the statistical significance of the differences of a dependent variable across two or more treatment groups [35]. Each dependent variable (Phi, Theta and Psi) was tested with Kruskal–Wallis on a 0.05 level of significance (p). The analysis was performed separately for the poses held in the area that was not magnetically disturbed and the area that was magnetically disturbed.

For the area which was not magnetically distorted, it was found that the distributions of both Phi and Theta were not significantly different across the 3 algorithms with $H(2) = 5.478$, $p = 0.065$ and $H(2) = 2.439$, $p = 0.295$, respectively. The (null) hypothesis that the distribution of orientation errors is the same across algorithms was rejected only for the Psi angle, for which $H(2) = 14.586$, $p = 0.001$. For the Psi errors, GMV-D and GMV-S had very similar mean ranks of 384.93 and 381.70, respectively, while KF had a larger mean rank, at 449.86. These analyses formally confirmed that, with respect to Phi and Theta, the performance of GMV-D, GMV-S or KF for orientation estimation in the magnetically undisturbed area was similar (i.e., not statistically different at a significance level of 0.05). Since that was not the case for the errors in the Psi angle, a closer look was taken by performing pairwise comparisons. Their results indicated that there are no statistically significant differences of the orientation errors in Psi between GMV-S and GMV-D ($p = 1.000$) while KF shows statistically significant differences of the orientation errors with both GMV-S ($p =$

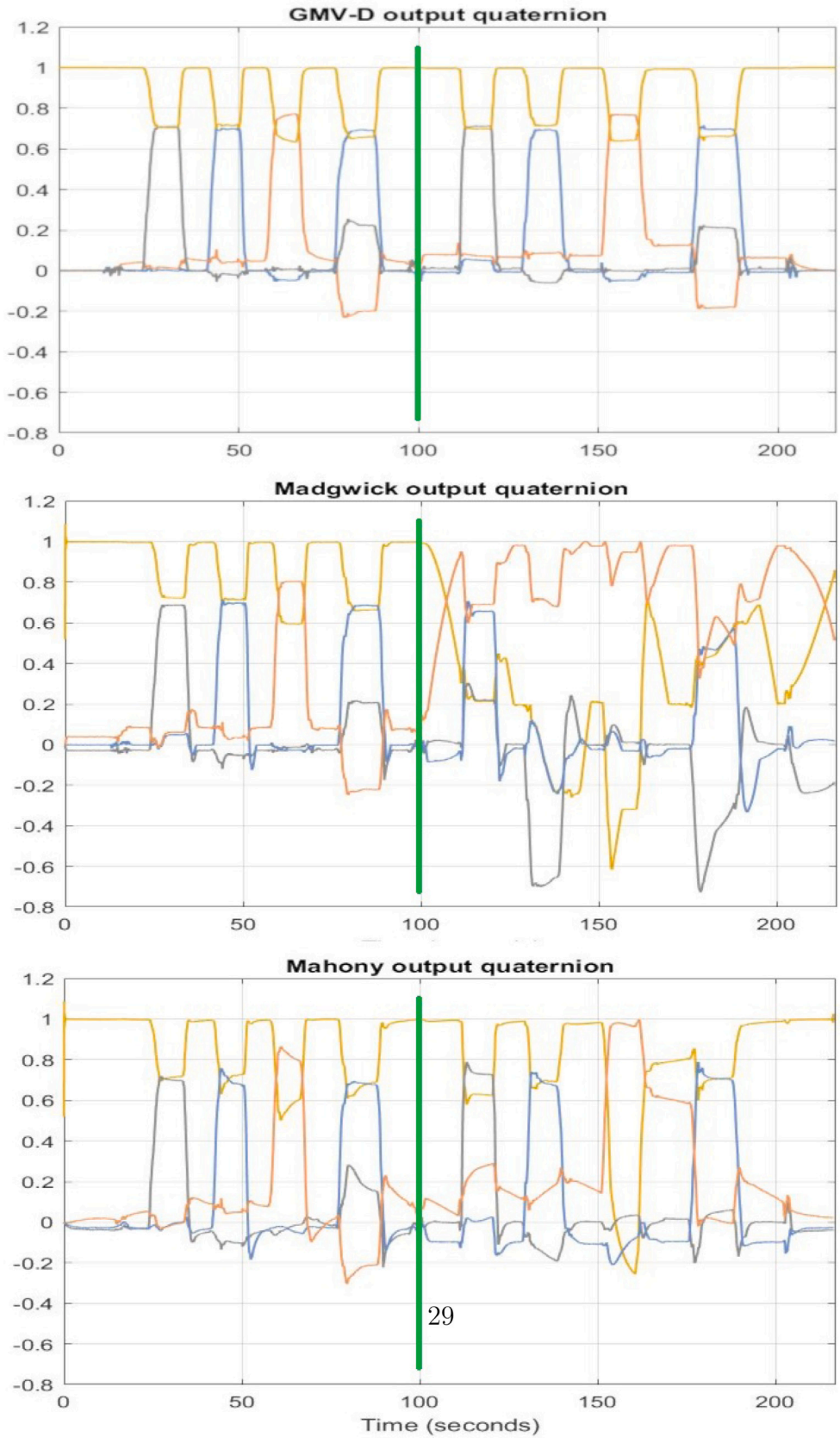

Fig. 7. Comparison of GMV-D, Madgwick and Mahony methods. (For interpretation of the references to color in this figure legend, the reader is referred to the web version of this article.)

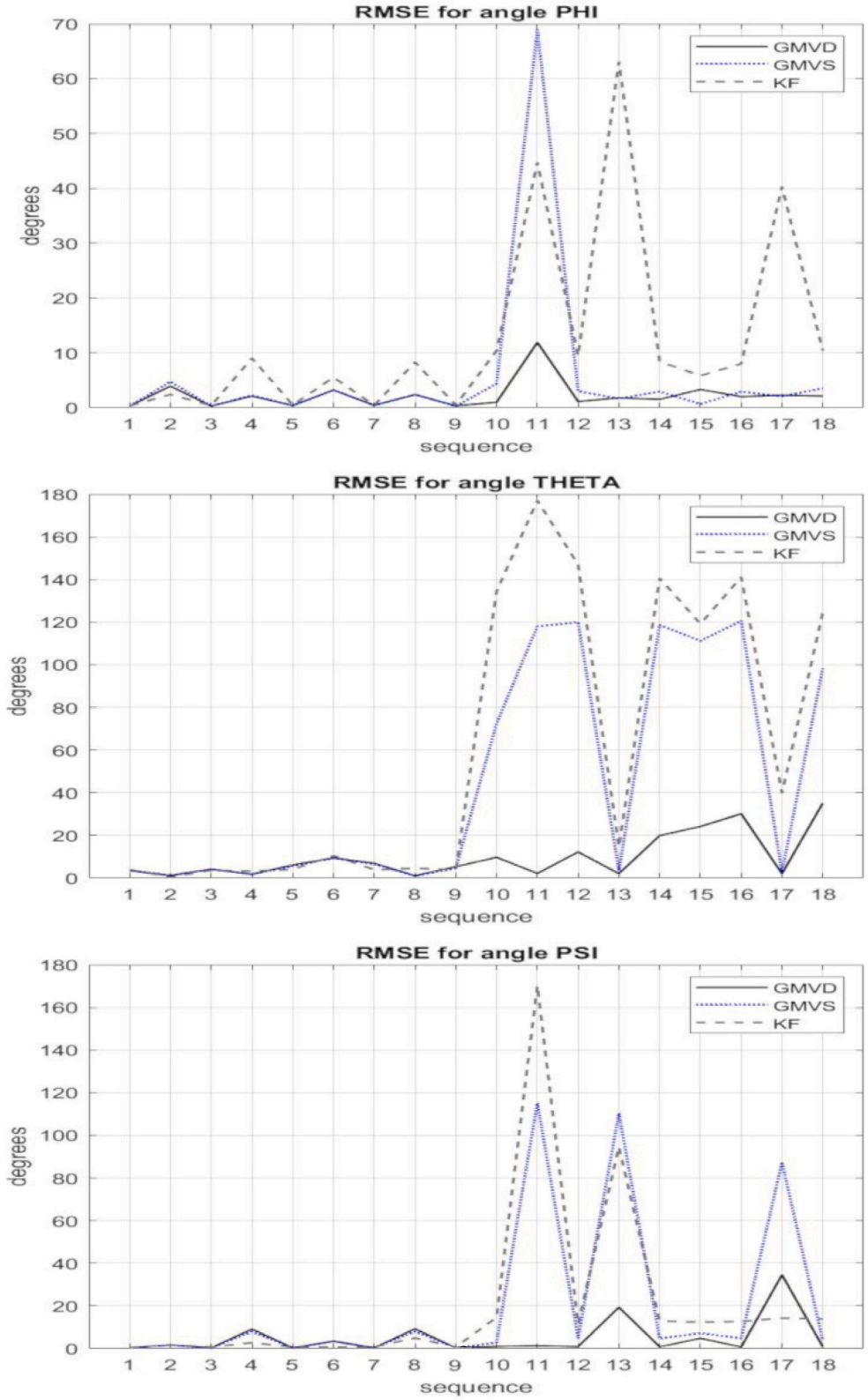

Fig. 8. Euler Angle RMSE values for GMV-D, GMV-S and KF. (For interpretation of the references to color in this figure legend, the reader is referred to the web version of this article.)

0.002) and GMV-D ($p = 0.004$). This is in agreement with the KF mean rank observed to be larger than the other two, which were very close among them.

For the magnetically distorted area, Table 5 shows the summary of the Kruskal–Wallis results for all three angles. The numbers under the headings GMV-D, GMV-S, and KF indicate the mean rank values

Table 5
Summary results of the Kruskal–Wallis tests in the magnetically distorted area.

Euler angle	H statistic, p value	GMV-D mean rank value	GMV-S mean rank value	KF mean rank value
Phi*	H(2) = 365.929, p = 0.000	252.20	342.62	621.69
Theta*	H(2) = 377.616, p = 0.000	197.76	432.47	586.27
Psi*	H(2) = 278.583, p = 0.000	229.84	421.93	564.73

for each of the orientation estimation methods, for the independent variable identified for each row.

The values of p for all 3 independent variables are very low, indicating that the corresponding (null) hypothesis that the errors generated by the 3 algorithms (treatments) are similar must be rejected ($p < 0.05$), which we denote with the asterisk. After finding that the errors from the 3 algorithms are not from the same distribution, it is important to observe that the mean rank values for GMV-D are the lowest (underlined), the values for GMV-S are intermediate and the values for KF are consistently the largest, in all 3 rows. For each independent variable (Phi, Theta and Psi), pairwise comparisons were performed and, in all three cases, it was found that the differences for the 3 possible pairs (GMV-D vs. GMV-S; GMV-D vs. KF ; GMVS vs. KF) are all significant with $p < 0.001$. All of these results confirm that the performance of GMV-D, GMV-S and KF in the magnetically distorted area was markedly different, with GMV-D yielding the lowest level of errors for all three Euler Angles. The results provide formal confirmation of the intuitive assessments that one might have derived from observation of the RMSE plots, shown in the 3 panels of Fig. 8.

3.7. GMV-D computation timing

When the evaluation with 30 human subjects was performed, all the computations (except for the Kalman Filter computations executed inside the MARG module) were performed in real-time by the same processor (the Intel Core i5 vPro, 3.4 GHz in the Dell Optiplex 990 desktop PC used for the initial implementation of the system). However, the same PC was also responsible for displaying the Unity sequence of animations provided as guidance to the subjects and collection of all the results to permanent storage for further analysis.

In order to assess the timing requirements of just the GMV-D computations, exclusively, we have modified the C♯ program running under Unity to record a timing mark in each iteration when the data from the sensors has been received and another when the GMV-D q_{OUT} quaternion has been computed. The difference between these timing marks reveals the time required to implement one iteration of the GMV-D algorithm.

Running the modified program on a contemporary desktop computer (Dell Vostro, with a 10th generation Intel Core i5-10400, 2.6 GHz) for 2400 iterations, we found that the GMV-D computations for each iteration took 24.85 ± 2.55 microseconds. Taking approximately 25 microseconds per iteration the computation time of GMV-D is appropriate for real-time performance at the sampling rates that are usually employed for hand tracking applications.

4. Discussion

The preceding section, overall, showed results that match the key intent of the development of GMV-D, which was to make the orientation estimation from MARG signals more robust in circumstances where distortions of the geomagnetic field exist.

The first half of the evaluation trials took place in a region of space where the geomagnetic field was not distorted (non-magnetically distorted area), whereas the second half took place in the immediate neighborhood of the iron bar, which was known to introduce significant distortion of the magnetic field (magnetically distorted area).

A plot of the 4 components of the orientation quaternions found by the 4 methods compared (Fixed Bias, Kalman Filter, GMV-S and GMV-D), for a complete representative trial is shown in Fig. 4. The Fixed Bias approach, is affected by drift throughout the complete trial. All 3 remaining algorithms seem to provide plausible orientation estimations during the first half of the experiment, displaying very similar evolutions of their quaternion outputs to the left of the green vertical dividing line in Fig. 4. In contrast, while the poses held after the subject translated the MARG module to the magnetically distorted zone (to the right of the green dividing line in Fig. 4) were exactly the same poses as previously executed in the non-magnetically distorted area, the quaternion outputs of KF and GMV-S do not appear similar to their outputs for the first half. This indicates that significant orientation estimation errors were introduced in the results from KF and GMV-S while at the magnetically distorted area. Only the bottom traces in Fig. 4, corresponding to GMV-D, appear to be essentially the same in the first and the second halves of the experiment, as they were expected to be. It is, however, not easy to perceive, in Fig. 4, the importance of the orientation errors suspected in the outputs from KF and GMV-S through the second half of the trial.

The 3D renderings in Figs. 5 and 6 provided intuitive confirmation of the resilience displayed by GMV-D for estimating the orientation of the MARG when the module was in the magnetically distorted area.

Figs. 4, 5 and 6 were created from orientation results during the completion of one representative trial, performed by one of the volunteer subjects. However, it was also necessary to evaluate the results accounting for the diversity of trajectories, movement speeds, etc. that various human subjects would use in completing the experimental task, as the system is meant to be part of a human–computer interface. To that end, 30 volunteer subjects were asked to perform the experimental protocol and the orientation results generated for all the poses in the trials were recorded. Only results from KF, GMV-S and GMV-D were subjected to this multi-user analysis. To investigate the deviations of the orientations estimated by each of the 3 methods from the "instructed orientations" ("ground truth") and in order to report the results in a more intuitive way, the orientation errors were expressed as errors in each one of the 3 Euler Angles. These angles (Phi, Theta, and Psi) are the angles rotated about the x, y, and z axes of the "body frame" of the module, and can, therefore, be more readily interpreted than the 4 numerical components of a quaternion. Ideally, the errors in the 3 Euler Angles would be 0. Thus, for a given pose, a lower error value found for one method than for another implies that the former performed better than the latter.

The root-mean-squared values (over the 30 subjects) of the error recorded for the 3 methods, at all 18 poses in the trial, are displayed separately for each of the Euler Angles in Fig. 8. This figure, and Table 4, clearly confirm that GMV-D incurred much lower RMSE levels than GMV-S and KF in the magnetically distorted area. This lends further support to the perceived increased resilience of GMV-D to estimate the orientation of the MARG when magnetic disturbances are present.

At this point, it was of interest to test if the apparent enhanced performance of GMV-D in the magnetically distorted area reached statistical significance. Due to the nature of the error data the non-parametric Kruskal–Wallis analysis of variance test was utilized to see if, in spite of their disparate means the error values from the 3 methods might still belong to the same distribution. (This would have meant that the errors from GMV-D were actually not statistically significantly different from the errors from GMV-S or KF). In accordance with the preliminary observations obtained (e.g., the shapes of the RMSE traces shown in Fig. 8), we performed the Kruskal–Wallis test separately for the errors recorded in the magnetically undisturbed area and for the

errors recorded in the magnetically distorted area. The analysis was performed for each of the 3 independent variables (i.e., the 3 Euler Angles).

The results detailed in Section 3.6 confirm the tentative conclusions derived from the RMSE values: In the magnetically undisturbed area the errors generated by KF, GMV-S, and GMV-D are not significantly different, with the exception for the angle Psi, where it was found that only KF was significantly different to GMV-S and GMV-D. But in the magnetically distorted area the errors from the 3 methods were statistically different (at a significance level p = 0.5). Additionally, all the pairwise comparisons were also significant, which implies that the lower mean rank values for GMV-D found in Table 5 do represent a better performance by this algorithm.

Although the additional comparison of GMV-D and the algorithms by Madgwick and Mahony (Section 3.3, Fig. 7) is limited in scope, it seems to also point to a more robust orientation estimation by GMV-D in the magnetically disturbed area. Furthermore, Fig. 7 indicates that GMV-D was less prone than other algorithms (e.g., Mahony's) to "overshooting" and exhibiting a slow progressive convergence during pose transitions. The avoidance of slow convergence in GMV-D may be due to the fact that this algorithm is set up to allow very strong accelerometer- and/or magnetometer-based corrections in every iteration if α and/or μ are high enough.

From the considerations presented above, we believe that the key contributions of the GMV-D algorithm are:

- Parallel and independent use of accelerometer and magnetometer readings to derive initial fully corrected improvements to the basic gyroscope-based orientation estimation
- Definition of practical scalar trustworthiness parameters that can be updated as frequently as every sample
- Simple algorithm that coalesces the 2 possible corrections to the gyroscopic orientation update involving each of them only to the extent justified by its trustworthiness parameter

These are all innovative features in the proposed GMV-D algorithm, which have resulted in significantly smaller levels of orientation error in the magnetically disturbed areas than the alternative methods used for comparison.

The implications of the enhanced performance of GMV-D are derived from the broadening of application scenarios that are feasible when MARG orientation estimation can take place even in the magnetically disturbed areas frequently found around everyday computer usage. Availability of resilient MARG orientation estimation methods, such as GMV-D, will facilitate the development of human–computer interfaces based on hand-tracking and mid-air gestures.

The GMV-D approach, of course, has several limitations. The initialization of the algorithm must be performed while the MARG module is static and in a magnetically undisturbed area, so that A_{int} and M_{int} are properly assigned at startup.

If any orientation offset exists at startup between the body frame of the MARG module and the inertial frame that the user wants to utilize, the offset (rotation) must be know and "added" to the q_{OUT} of every iteration through a rotation-compounding operation, similar to Eq. (7). (This can be avoided by placing the MARG body frame in alignment with the desired inertial frame at startup).

Similarly, GMV-D estimates the orientation of (the body frame of) the MARG module and has no internal provisions to account for any orientation offset that may exist between the MARG body frame and the rigid body (e.g., body segment) that it might be attached to. Assessment and post-compensation of such orientation offset would need to be implemented outside the GMV-D algorithm itself.

An additional limitation that is inherent to the definition of the GMV-D algorithm is that the implementation of strong accelerometer- and/or magnetometer-based corrections will take place at unknown intervals. This is because GMV-D will only allow strong corrections to be applied if the corresponding parameters (α and/or μ) have a high value. This is perhaps, one of the leading factors that could, potentially, degrade the performance of the GMV-D orientation estimation algorithm, for prospective application scenarios where the MARG remains in non-uniform movement for long intervals (so that α does not get to reach high levels) and simultaneously is located in magnetically disturbed areas, (so that μ does not get to reach high levels). Under those circumstances, GMV-D will, as expected, prevent the implementation of strong accelerometer- or magnetometer-based corrections (which is a defensive mechanism to prevent the implementation of costly erroneous corrections). If that were the case, the potential growth of drift in the orientation estimate driven by integration of the outputs of the gyroscope would not be significantly corrected during those intervals, resulting in a progressive deterioration in the orientation estimate accuracy. Fortunately, the constraints expected when the MARG is embedded in the glove worn by a computer user (Section 1.1) are likely to permit the frequent application of strong accelerometer- and magnetometer-based corrections, if they are needed.

5. Conclusions and future work

We aimed to create a robust system that can determine, in real-time, the correct orientation of a MEMS MARG module so that multiple MARG modules can be embedded in an instrumented glove that will report the real-time position, orientation, and configuration of the hand of a computer user, enabling new avenues for hand-gesture-based human–computer interaction.

When MEMS MARG modules were initially introduced, there were hopes that these devices could be used for determining orientation and position in ways similar to the use of their large-scale counterparts for aircraft navigation. However, it was soon found that the much poorer performance characteristics of the MEMS sensors prevented the direct use of the same processing approaches as used for larger devices. In particular, as the output of the gyroscopes must be integrated to calculate orientation, even small levels of gyroscope offset will cause high levels of "drift" error in the orientation estimation. Further, this error will tend to rapidly and linearly grow with respect to time. Designers have sought to apply frequent corrections to the orientation calculated from the signals of the gyroscope using information from the accelerometer and, more recently, from MEMS magnetometers, when they began to be included in the sensor packages. However, accelerometer corrections should only be applied when the module is static so that the accelerometer reports only the acceleration of gravity, and magnetometer corrections should only be applied if the local geomagnetic field measured by the device is not distorted due to the presence of nearby ferromagnetic objects.

The new processing approach we propose strives to achieve real-time robust orientation estimation for a typical MARG module in the context of human–computer interaction. This context implies that a 3-camera IR-video system can be used to determine the approximate position of the MARG module, which enabled the novel idea of mapping the level of magnetic trustworthiness (encoded in a parameter $0 \leq \mu \leq 1$) of small regions of the working space of the device. This is used to reduce the weight given to the magnetic correction component where the magnetic field is distorted, enhancing the robustness of the system.

Two distinct advantages of the GMV-D approach are, first that it does not require the user to set any initialization parameters (as other approaches, such as the Kalman Filter require), and second, that it implements processing pipelines where the information derived from the three sensing modalities available in the MARG module (gyroscope, accelerometer, and magnetometer) are kept independent and separately accessible throughout most of each algorithm iteration. This is in contrast to other approaches which might "fuse" or "mix" the several sources of information early-on in the algorithm. This parallel management of the information from the sensors allows a more explicit comparison between them or even a retrospective analysis for each of

them, such that additional mechanisms for suppressing the influence of a sensing modality that is displaying incongruent behavior may be implemented.

In summary, it is likely that the contributions of the GMV-D method may help in making the MARG orientation estimation process more robust by fully taking advantage of the MARG operating conditions for a typical human–computer interaction application and comprehensively utilizing all the sensing modalities available in the MARG module.

The parallel processing pipelines that keep the information from the accelerometer and the magnetometer independent throughout each iteration of the GMV-D algorithm may provide an alternative mechanism to detect when the local magnetic field is likely distorted, based exclusively on the internal signals from the MARG module. In the current version of GMV-D, the local magnetic trustworthiness parameter, μ, is defined by "mapping" the regions of space that have been previously visited by the MARG module. The "mapping" process makes use of the position estimates provided by the IR-camera system. This is completely acceptable for the intended use of the MARG module, as part of a hand-tracking system meant for human–computer interaction. However, finding an alternative mechanism for the detection of magnetic field alterations, utilizing only the signals generated by the MARG module, would extend the scope of use of the algorithm. This would be very significant, for example, to enable the use of the GMV-D orientation estimation method in ambulatory applications (such as gait studies performed during everyday activities of the subject) where position estimates may not be readily available.

Similarly, the accuracy level reached by the GMV-D method may be increased if a higher-level management of the trustworthiness parameters, α and μ, is implemented dynamically. For example, the current system updates the μ value for any visited voxel by merely replacing the value with the newest calculation of μ. This was implemented so that, even if the ferromagnetic objects in the working space of the system were occasionally shifted, the system would keep an updated μ map that can reflect those infrequent changes. To enhance the accuracy of the system, however, it may be beneficial to keep track of the last few (e.g., 3 or 5) values of μ calculated for a given voxel, assigning a latency-weighted mean of those few values in the update of the voxel.

CRediT authorship contribution statement

Neeranut Ratchatanantakit: Software, Formal analysis, Methodology, Validation, Investigation, Writing – original draft. **Nonnarit O-larnnithipong:** Software, Methodology. **Pontakorn Sonchan:** Software, Data curation. **Malek Adjouadi:** Resources, Supervision. **Armando Barreto:** Conceptualization, Writing – review & editing, Supervision.

Declaration of competing interest

The authors declare that they have no known competing financial interests or personal relationships that could have appeared to influence the work reported in this paper.

Acknowledgments

National Science Foundation, United States grants CNS-1532061 and CNS-1920182, FIU University Graduate School Dissertation Year Fellowship, United States for Dr. Neeranut Ratchatanantakit.

Appendix

Quaternion That Represents a Rotation Between Two Vectors ($\vec{a}$ and $\vec{b}$)

$$\vec{a}\times\vec{b} = \|\vec{a}\|\|\vec{b}\|sin(2\theta)\vec{n} \tag{A.1}$$

$$\vec{a}\times\vec{b} = 2\|\vec{a}\|\|\vec{b}\|sin(\theta)cos(\theta)\vec{n} \tag{A.2}$$

$$\vec{a}\times\vec{b} = [2\|\vec{a}\|\|\vec{b}\|cos(\theta)]sin(\theta)\vec{n} \tag{A.3}$$

$$\vec{a}\cdot\vec{b} = \|\vec{a}\|\|\vec{b}\|cos(2\theta) \tag{A.4}$$

$$\vec{a}\cdot\vec{b} = \|\vec{a}\|\|\vec{b}\|(2cos^2(\theta)-1) \tag{A.5}$$

$$\vec{a}\cdot\vec{b} = 2\|\vec{a}\|\|\vec{b}\|cos^2(\theta) - \|\vec{a}\|\|\vec{b}\| \tag{A.6}$$

$$\vec{a}\cdot\vec{b} + \|\vec{a}\|\|\vec{b}\| = [2\|\vec{a}\|\|\vec{b}\|cos(\theta)]cos(\theta) \tag{A.7}$$

For ease of calculation, the term $[2\|\vec{a}\|\|\vec{b}\|cos(\theta)]$ in Eqs. (A.1)–(A.7) is substituted by a variable m.

Let $m = 2\|\vec{a}\|\|\vec{b}\|cos(\theta)$

$$\vec{a}\times\vec{b} = (m)\vec{n}sin(\theta) \tag{A.8}$$

$$\vec{a}\cdot\vec{b} + \|\vec{a}\|\|\vec{b}\| = (m)cos(\theta) \tag{A.9}$$

Since $\vec{a}\times\vec{b}$ is a three-dimensional vector and $\vec{a}\cdot\vec{b}+\|\vec{a}\|\|\vec{b}\|$ is scalar, therefore, a quaternion q' can be constructed from these components, as shown in Eq. (A.10). Eq. (A.11) shows the calculation for the norm of quaternion q'. Since $\vec{n}$ is a unit vector, then its norm squared $(n_x^2+n_y^2+n_z^2)$ equals to 1. Therefore, we can conclude as shown in Eq. (A.11) that $\|q'\| = m$.

$$q' = \mathcal{H}(\vec{a}\times\vec{b}, \vec{a}\cdot\vec{b} + \|\vec{a}\|\|\vec{b}\|) = (m)\vec{n}sin(\theta) + (m)cos(\theta) \tag{A.10}$$

$$\|q'\| = \sqrt{(m)^2[(sin^2(\theta))(n_x^2+n_y^2+n_z^2) + cos^2(\theta)]} = m \tag{A.11}$$

$$q = \frac{q'}{\|q'\|} = \vec{n}sin(\theta) + cos(\theta) \tag{A.12}$$

Eq. (A.12) satisfies the definition of a unit quaternion that represents the rotation of angle 2θ about $\vec{n}$. Therefore, the quaternion $q = \frac{q'}{\|q'\|}$ can be used to describe the angular difference between vectors $\vec{a}$ and $\vec{b}$, where

$$q' = \vec{a}\times\vec{b} + (\vec{a}\cdot\vec{b} + \|\vec{a}\|\|\vec{b}\|) \tag{A.13}$$

References

[1] S.J.J. Kim, A user study trends in augmented reality and virtual reality research: A qualitative study with the past three years of the ismar and ieee vr conference papers, in: 2012 International Symposium on Ubiquitous Virtual Reality, IEEE, 2012, pp. 1–5.

[2] E. Foxlin, et al., Motion tracking requirements and technologies, in: Handbook of Virtual Environment Technology, Vol. 8, 2002, pp. 163–210.

[3] M. Nazarahari, H. Rouhani, 40 Years of sensor fusion for orientation tracking via magnetic and inertial measurement units: Methods, lessons learned, and future challenges, Inf. Fusion 68 (2021) 67–84, http://dx.doi.org/10.1016/j.inffus.2020.10.018.

[4] F.L. Markley, D. Mortari, Quaternion attitude estimation using vector observations, J. Astronaut. Sci. 48 (2000) 359–380, http://dx.doi.org/10.1007/BF03546284.

[5] W.H.K. de Vries, H.E.J. Veeger, C.T.M. Baten, F.C.T. van der Helm, Magnetic distortion in motion labs, implications for validating inertial magnetic sensors, Gait & Posture (ISSN: 0966-6362) 29 (4) (2009) 535–541, http://dx.doi.org/10.1016/j.gaitpost.2008.12.004, (https://www.sciencedirect.com/science/article/pii/S0966636208003858).

[6] M. Nazarahari, H. Rouhani, Sensor fusion algorithms for orientation tracking via magnetic and inertial measurement units: An experimental comparison survey, Inf. Fusion 76 (2021) 8–23, http://dx.doi.org/10.1016/j.inffus.2021.04.009.

[7] A.M. Sabatini, Quaternion-based extended kalman filter for determining orientation by inertial and magnetic sensing, IEEE Trans. Biomed. Eng. 53 (7) (2006) 1346–1356, http://dx.doi.org/10.1109/TBME.2006.875664, URL https://ieeexplore.ieee.org/document/1643403.

[8] M.-D. Hua, G. Ducard, T. Hamel, R. Mahony, K. Rudin, Implementation of a nonlinear attitude estimator for aerial robotic vehicles, IEEE Trans. Control Syst. Technol. 22 (1) (2014) 201–213, http://dx.doi.org/10.1109/TCST.2013.2251635, URL https://ieeexplore.ieee.org/document/6516072.

[9] J. Justa, V. Šmídl, A. Hamáček, Fast ahrs filter for accelerometer, magnetometer, and gyroscope combination with separated sensor corrections, Sensors (Basel, Switzerland) 20 (14) (2020) 3824, http://dx.doi.org/10.3390/s20143824, URL https://search.proquest.com/docview/2423395953.

[10] A. Harindranath, M. Arora, Mems Imu Sensor Orientation Algorithms-Comparison in a Simulation Environment, IEEE, 2018, pp. 1–6, http://dx.doi.org/10.1109/ICNEWS.2018.8904029, URL https://ieeexplore.ieee.org/document/8904029.

[11] S.O.H. Madgwick, An efficient orientation filter for inertial and inertial/magnetic sensor arrays, 2010.

[12] R. Mahony, T. Hamel, J.M. Pflimlin, Complementary Filter Design on the Special Orthogonal Group SO(3), IEEE, 2005, pp. 1477–1484, http://dx.doi.org/10.1109/CDC.2005.1582367, URL https://ieeexplore.ieee.org/document/1582367.

[13] R.E. Kalman, A new approach to linear filtering and prediction problems, J. Basic Eng. 82 (1) (1960) 35–45, http://dx.doi.org/10.1115/1.3662552.

[14] A. Barreto, M. Adjouadi, F.R. Ortega, N. O-larnnithipong, Intuitive Understanding of Kalman Filtering with MATLAB®, CRC Press, 2020.

[15] J.L. Marins, X. Yun, E.R. Bachmann, R.B. McGhee, M.J. Zyda, An extended kalman filter for quaternion-based orientation estimation using marg sensors, in: Proceedings 2001 IEEE/RSJ International Conference on Intelligent Robots and Systems. Expanding the Societal Role of Robotics in the Next Millennium (Cat. No. 01CH37180), Vol. 4, IEEE, 2001, pp. 2003–2011, http://dx.doi.org/10.1109/IROS.2001.976367, URL https://ieeexplore.ieee.org/document/976367.

[16] L. Peppoloni, A. Filippeschi, E. Ruffaldi, C.A. Avizzano, A Novel 7 Degrees of Freedom Model for Upper Limb Kinematic Reconstruction Based on Wearable Sensors, IEEE, 2013, pp. 105–110, http://dx.doi.org/10.1109/SISY.2013.6662551, URL https://ieeexplore.ieee.org/document/6662551.

[17] Yost Labs, 3-space sensor miniature attitude and heading reference system with pedestrian tracking user's manual, 2007-2017, URL https://yostlabs.com/wp/wp-content/uploads/pdf/3-Space-Sensor-Users-Manual-3.pdf.

[18] P. Yost, Yost Labs, Qgrad vs. Kalman filter. URL https://yostlabs.com/about/feature-advantages/qgrad-vs-kalman-filter/.

[19] H. Himberg, Y. Motai, C. Barrios, R-adaptive kalman filtering approach to estimate head orientation for driving simulator, in: 2006 IEEE Intelligent Transportation Systems Conference, 2006, pp. 851–857, http://dx.doi.org/10.1109/ITSC.2006.1706850.

[20] D. Roetenberg, H.J. Luinge, C.T.M. Baten, P.H. Veltink, Compensation of magnetic disturbances improves inertial and magnetic sensing of human body segment orientation, IEEE Trans. Neural Syst. Rehabil. Eng. 13 (3) (2005) 395–405, http://dx.doi.org/10.1109/TNSRE.2005.847353, URL https://ieeexplore.ieee.org/document/1506825.

[21] P. Daponte, L.D. Vito, S. Rapuano, M. Riccio, F. Picariello, Compensating Magnetic Disturbances on Marg Units by Means of a Low Complexity Data Fusion Algorithm, IEEE, 2015, pp. 157–162, http://dx.doi.org/10.1109/MeMeA.2015.7145191, URL https://ieeexplore.ieee.org/document/7145191.

[22] P. Daponte, L.D. Vito, G. Mazzilli, F. Picariello, S. Rapuano, Method for Compensating the Effect of Disturbances on Magnetometer Measurements: Experimental Results, IEEE, 2017, pp. 1–6, http://dx.doi.org/10.1109/I2MTC.2017.7969980, URL https://ieeexplore.ieee.org/document/7969980.

[23] J. Wu, Real-time magnetometer disturbance estimation via online nonlinear programming, IEEE Sens. J. 19 (12) (2019) 4405–4411, http://dx.doi.org/10.1109/JSEN.2019.2901925, URL https://ieeexplore.ieee.org/document/8653903.

[24] R.G. Valenti, I. Dryanovski, J. Xiao, Keeping a good attitude: a quaternion-based orientation filter for imus and margs, Sensors (Basel, Switzerland) 15 (8) (2015) 19302–19330, http://dx.doi.org/10.3390/s150819302, URL https://www.ncbi.nlm.nih.gov/pubmed/26258778.

[25] K. Shoemake, Animating rotation with quaternion curves, in: Proceedings of the 12th Annual Conference on Computer Graphics and Interactive Techniques, 1985, pp. 245–254.

[26] E.B. Dam, M. Koch, M. Lillholm, Quaternions, Interpolation and Animation, Vol. 2, Citeseer, 1998.

[27] N. O-larnnithipong, A. Barreto, S. Tangnimitchok, N. Ratchatanantakit, Orientation correction for a 3d hand motion tracking interface using inertial measurement units, in: International Conference on Human-Computer Interaction, Springer, 2018, pp. 321–333.

[28] M. De Franceschi, D. Zardi, Evaluation of cut-off frequency and correction of filter-induced phase lag and attenuation in eddy covariance analysis of turbulence data, Bound.-Lay. Meteorol. 108 (2) (2003) 289–303, http://dx.doi.org/10.1023/A:1024157310388, URL https://search.proquest.com/docview/737537706.

[29] J. Meyer, K. Padayachee, B.A. Broughton, A robust complementary filter approach for attitude estimation of unmanned aerial vehicles using ahrs, criticizes and develops further Valenti's approach, 2019.

[30] S. Qiu, H. Zhao, N. Jiang, Z. Wang, L. Liu, Yi. An, H. Zhao, X. Miao, R. Liu, G. Fortino, Multi-sensor information fusion based on machine learning for real applications in human activity recognition: State-of-the-art and research challenges, Inf. Fusion 80 (C) (2022) 241–265, http://dx.doi.org/10.1016/j.inffus.2021.11.006.

[31] G. Marta, F. Simona, C. Andrea, B. Dario, S. Stefano, V. Federico, B. Marco, B. Francesco, M. Stefano, P. Alessandra, Wearable biofeedback suit to promote and monitor aquatic exercises: A feasibility study, IEEE Trans. Instrum. Meas. 69 (4) (2020) 1219–1231, http://dx.doi.org/10.1109/TIM.2019.2911756.

[32] J.B. Kuipers, Quaternions and Rotation Sequences: A Primer with Applications to Orbits, Aerospace, and Virtual Reality, Princeton University Press, 1999.

[33] A.J. Hanson, Visualizing quaternions, in: ACM SIGGRAPH 2005 Courses, 2005, pp. 1–es.

[34] D.C. Montgomery, Design and Analysis of Experiments, John wiley and sons, 2017.

[35] A. Field, Discovering Statistics using SPSS, Sage publications, 2009.